Accelerating Cleanup of the Defense Nuclear Legacy

Quarterly Technical Progress Report
for the period
October 1, 2008 – December 31, 2008

Dr. W. Glenn Steele, Interim Principal Investigator

Report No. 07040R08

Prepared for the U.S. Department of Energy
Agreement No. DE-FC01-06EW-07040

Institute for Clean Energy Technology
Mississippi State University
205 Research Boulevard
Starkville, MS 39759

icet@icet.msstate.edu
www.icet.msstate.edu

Acknowledgement
This material is based upon work supported by the Department of Energy under award number DE-FC01-06EW-07040

Table of Contents

EXECUTIVE SUMMARY *1*

Task 1. Modeling and Experimental Support for High-Level SRS Salt Disposition Alternatives **4**

Task 2. Process Improvements of the Defense Waste Processing Facility (DWPF) **15**

Task 3. High Efficiency Particulate Air (HEPA) **22**

Task 4. Support of Hanford Single Shell Tank Waste Disposition **23**

Task 5. Long-Term Monitoring of Selected Heavy Metal and Radionuclide Contaminants and Application of Phytoremediation **38**

Task 6 . Saltstone **43**

Task 7 . Bioavailability studies of mercury and other heavy metal contaminants in ecosystems of selected DOE sites **47**

Task 8. Hanford Tank Inspection **51**

List of Figures

Figure 1. Mass spectroscopy spectra of organic layer in methylene chloride 5

Figure 2. PLM image of crystals found in emulsion layers 6

Figure 3. ESP flowsheet for mixing of the 0.05 M HNO_3 scrub solution with a portion of the aqueous phase of the simulant 7

Figure 4. Effect of simulant carry-over in the 0.05 M HNO_3 scrub solution 8

Figure 5. Comparison of ESP pH predictions, Figure-4, with measured pH values (meter and indicator paper) 9

Figure 6. Variation of the pH as a foundation of carry over for three streams originating at different dissolution stages from SRS Tank 25F 10

Figure 7. The effect of pH from mixing the aqueous phase transfer streams with the nitric acid scrub solution on the resulting solids loading. 11

Figure 8. Variation of the main solids predicted by the simulations (Gibbsite and Dawsonite) as a function of pH 12

Figure 9. LIBS experimental setup for slurry sampling on substrate 16

Figure 10. LIBS signal variation with time. The data were obtained from slurry on a filter paper 17

Figure 11. Double-pulse LIBS experimental setup using a compact broadband spectrometer 18

Figure 12. Intensity variation of Mg lives at various interpulse dealy in DP-LIBS of Al Sample with a) broadband Mechelle 5000 spectrometer and b) Czerny-Turner spectrometer 19

Figure 13. Part of a double pulse LIBS spectra from 55% Ce O_2-batch pellet recorded at different inter-pulse delay times.....20

Figure 14. Total Volume of AY-101 during retrieval of C tanks 27

Figure 15. AY-101 Conditions during retrieval of C tanks 27

Figure 16. Total Volume of flush stream to AY tank 28

Figure 17. Conditions of Flush Stream to AY tank 28

Figure 18. AY-101 Solids (gmoles) 29

Figure 19. AY-101 Solids (gmoles)......29

Figure 20. Total Volume of AZ-101 during retrieval of C tanks 32

Figure 21. AZ-101 conditions during retrieval of C tanks 33

Figure 22. Total volume of flush stream to AZ tank. 33

Figure 23. Conditions of Flush Stream to AZ tank 34

Figure 24. AZ-101 Solids (gmoles) 34

Figure 25. AZ-101 Solids (gmoles) 35

Figure 26. Kinetics of Hg uptake by watter lettuce from solutions with initial Hg concentrations from 1 to 10 mg/L 39

Figure 27. Hg concentrations in shoots and roots as a function of Hg concentration in solution 40

Figure 28. Effects of Hg on a fresh weight of shoots and relative water contents....41

Figure 29. Absolute Thermocouple Measurements in Calorimeter 45

Figure 30. Differential temperature between sample and water bath. 45

Figure 31. Effects of initial pH on SO_4 and Fe release from pure HgS after reacting with Fe3O4 (1 gFe oxide, 0.1 g HgS, 35 ml 0.01 M NaNO3 at pH 4.0, 6.0 and 8.0 for 24 hours). 48

Figure 32. Final pH of pure HgS systems and HgS+Fe oxides at various initial pHs (conditions at the same as Fig. 1)....48

Figure 33. Effect of intial pH on sulfate release from Hg contaminated Oak Ridge soil (with 2000 mg/kgHg as HgS) (5g soil, 0.25gFe oxide, 35 ml 0.01 M $NaNO_3$ at pH 4.0, 6.0, and 8.0 for 24 hours) 49

Figure 34. Final pH of contaminated HgS Oak Ridge soil with two iron oxides under various initial pH (4.0-8.0) conditions 49

Figure 35. The net pH changes of contaminated soils after reacting with two iron oxides under various intial pHs....50

Figure 36. (a) Photograph of ICET FTP components on optical rail viewing non-descript, grey targets on white background at distance of 16.2 m (53') and angle of ~ 62°. A cloth shroud has been placed over the light source to minimize the amount of non-fringe pattern light on the target. (b) Example image of a non-descript target with fringe lines projected on its surface, acquired using the setup in (a). (c) ICET FTP components on optical rail as utilized in the setup in (a).. 53

Figure 37. Plot of the magnitude of the average absolute error divided by the true volume (giving the average relative error) as a function of the camera-to-projector distance d. Horizontal dithering has been applied to the data to separate the data points and 95% confidence-limit error bars 54

List of Tables

Table 1. ICP results (μg/mL) from aqueous layer of HBXX025 ..... *5*

Table 2. Composition (mol/L) of the SRS simulant employed in the Parsons Testing *7*

Table 3. Solids distribution and loading (g) for some of the simulations associated with the carry over of 25F transfer stream 4 to the CSSX scrub solution *11*

Table 4. The composition of the CeO2 batch pellet used in the test *20*

Table 5. AY tank and flush conditions during retrieval of C-107, C-101, and C105 ..... *25*

Table 6. AY-101 solids during the retrieval of C-107, C-101, and C-105 ..... ***Error! Bookmark not defined.***

Table 7. C tank conditions during retrieval into AY-101 ..... *30*

Table 8. AZ tank and flush conditions during retrieval of C-102. ..... ***Error! Bookmark not defined.***

Table 9. AZ-101 solids during the retrieval of C-102 ..... *32*

Table 10 . C-tank conditions during retrieval into AZ-101 ..... *35*

Table 11. C-111 initial composition change as NaOH is increased *36*

Table 12. C-111 initial composition change as NaOH is increased *37*

Table 13. Comparison of FTP-determined ("measured") and true volumes for three different non-descript targets. Each target was recorded in four different rotational orientations. The separation between camera and projector was 46.1 cm (~ 18"). *54*

Table 14. Comparison of average absolute errors for the selected non-descript targets as a function of the camera-to-projector distance ("baseline") d for d = 21.8 (~9"), d=33.4 cm (~13"), and d = 46.1 cm (~18"). The uncertainties are one standard deviation. In the laste column, the average of the absolute errors are presented *54*

Table 15. Comparison of average relative errors for the selected non-descript targets as a function of the camera-to-projector distance ("baseline") d for d = 21.8 cm (~9"), d = 33.4 cm (~ 13"), and d = 46.1 cm (~18"). In the last column, the average of the absolute values of the relative errors are presented *55*

EXECUTIVE SUMMARY

Task 1. Support of SRS Salt Disposition

Results from the remaining sample HBXX025 emulsion are presented. Three layers were present upon sample receipt: an organic, emulsion, and aqueous portion. All layers were evaluated and the emulsion appears to be predominantly organic in phase with a small amount of solid entrapped. A letter report will be sent to site personnel on all samples and data results.

ESP simulations on the effect of waste compositions on the carry over of waste into the nitric acid scrub solution employed in the CSSX process are reported. Model calculations have been carried out for recent experiments conducted at Parsons Engineering and indicated that the predominant solids predicted to re-precipitate were Gibbsite and Natrolite. Trends in pH were similar for the experiments and calculations and it is hoped that additional samples can be obtained which will validate the solids speciation. Simulations associated with downstream processing effects for dissolution fractions (transfer streams) from waste contained in SRS tank 25F are also given. In this case, the trend in pH is similar to that observed at Parsons; however, the function is shifted based on the input waste composition. A competition between Gibbsite and Dawsonite was predicted. Total solids loadings are expected to remain at less than 0.07% by weight indicating that only limited fouling should be expected.

Task 2. Process Improvements for the Defense Processing Facility (DWPF)

Laser induced breakdown spectroscopy (LIBS) is a diagnostic technique that can measure the concentrations of various elements in a test sample. This project evaluates LIBS as an on-line, simultaneous multi-species analysis of the slurry sample for Defense Waste Processing Facility. During this work period, a new compact broadband spectrometer was setup with double-pulse laser system to record LIBS data. LIBS data recorded with this system were compared with the data recorded with a Czerny-Turner spectrometer. LIBS experiments of DWPF slurry continued. We are evaluating a slurry sampling method which uses a substrate to hold slurry sample.

Task 3. High Efficiency Particulate Air (HEPA)

Activities associated with autopsying loaded filters to evaluate patterns of buildup on the surface of filter media as a function of aerosol challenge will be completed during the 4th quarter of 2008. A test plan will be developed for the process of evaluating excursions below safety design basis. A new series of investigations will be planned to identify the range of upset conditions encountered by HEPA filters that would not automatically result in their replacement. Additional efforts will be made to identify alternate funding sources for continuation of ICET's HEPA filter research program.

Task 4. Support of Hanford Single Shell Tank Waste Disposition

Development of a neural network to augment the chemistry in HTWOS, specifically for the C tank farm retrieval continued. An ESP program process model using the Modified Sluicing with Recycle (MSwR) and the Mobile Retrieval System (MRS) was used to simulate the retrieval of waste from C-107, C-101, and C-105 into AY-101, as well as, the retrieval of C-102 into AZ-101. In addition, the prediction by the ESP simulation program of a low pH value for the best basis initial C-111 composition was evaluated. It was determined that no basis for the adjustment of the C tank composition was available.

Task 5. Long-Term Monitoring of Selected Heavy Metal and Radionuclide Contaminants and Application of Phytoremediation

During this quarter, we conducted greenhouse studies on uptake of Hg by an aquatic plant species– Water Lettuce (*Pistia stratiotes*). The initial results show that water lettuce can effectively remove Hg from the solution and Hg was mostly stored in plant roots. One day of growing could remove 93-98% of Hg from solutions. However, Hg shows acute toxicity to water lettuce as indicated by decreases in fresh biomass and moisture contents.

Task 6. Saltstone

This project is designed to assist the Savannah River Site (SRS) in the production of the Saltstone waste form from low-level tank waste. The expectation of increased aluminum content in the next batch has raised concerns about an excess heat of hydration, which may create problems for the storage of the waste form. The facility also relies on vault temperature modeling to protect vault temperature limits. These studies are designed to examine the effects of the heat created by the reactions and to discover methods for either dealing with the excess heat or preventing it from occurring in the first place.

Task 7. Bioavailability Studies of Heavy Metals and Radionuclides Contaminants in Ecosystems of Selected DOE Sites

During this quarter, experiments were conducted on potential effects of pH on oxidation of HgS contaminated Oak Ridge soils by two common iron oxides (Fe_2O_3 and Fe_3O_4). The results show that pH did not significantly affect oxidation rates (SO_4 concentration) in HgS contaminated Oak Ridge soil and the Oak Ridge soil had a strong pH buffer capacity.

Task 8. In-Tank Characterization for Closure of Hanford Waste Tanks

Funds became available in September to perform a technical feasibility study for the Fourier profilometry (FTP) technique. This study and the report that will result were requested by our

Hanford collaborators before the budget reduction froze this effort. During this reporting period, FTP experiments were performed in the ICET highbay at distances and at angles of view that pertain to Hanford waste tanks. A preliminary analysis of the data has been completed and an uncertainty analysis of the FTP results is underway. Additional experiments are planned to help identify and characterize a systematic error.

Task 1

Support of SRS Salt Disposition

Jeffrey S. Lindner and Laura T. Smith

INTRODUCTION

Major needs in the SRS tank farms are dictated by the desire to separate actinides and cesium from salt wastes permitting the processing of the high activity waste fraction in the Defense Waste Processing Facility (DWPF) and stabilization of the lower activity waste as saltstone. Towards this end, efforts are currently underway for the development of the Salt Waste Processing Facility (SWPF) containing the Actinide Removal Process (ARP) and Caustic Side Solvent Extraction Unit (CSSX).[1-3] Current progress involves the pilot-scale testing of the CSSX process wherein solids re-precipitation and emulsions formation has been observed within the contactors and in wash and scrub liquors.

In addition the processing of sludge (caustic addition to Batch 5) to reduce the fraction of aluminum routed to the DWPF is scheduled for FY'08. [4-6]. It is expected that aluminum-rich supernatants will be processed in the same manner as salt waste. Here, however, the downstream implications of mixing the aluminum-rich supernatant with DDA fractions from salt waste retrieval and other streams such as the DWPF recycle are unknown. The silicon concentration within the DWPF recycle stream along with the high aluminum loading in the Batch 5 (and potentially other sludge batches) leachate may indicate the formation of intractable aluminosilicates which will create a downstream problem owing to negligible solubility and the propensity for co-precipitation of uranium.

This project is divided into 2 Tasks. Task 1.1 is aimed at evaluation of the CSSX process through experiments and thermodynamic modeling. In collaboration with Parsons Engineering, the analysis of solids and scales observed in various portions of the process, including contactors, filters and solids formed in drain tanks. These solids will be analyzed using x-ray diffraction and inductively coupled plasma emission spectroscopy. Laboratory kinetic experiments are also planned to examine the stability of simulants to be used in pilot-scale testing at Parsons.

Task 1.2 is aimed at assessing stream stability for blended compositions arising from potential tank farm operations. Any stream blending will be performed upstream of the SWPF. The primary streams of concern are the DWPF Recycle stream, which consists of DWPF overheads and is routed to the tank farm, high aluminum concentration streams from sludge leaching operations (50% NaOH) and dissolved salt streams originating from saltcake dissolution. Predicted compositions will be assessed through calculated parameters such as percent solids by weight, aqueous phase density, adherence to corrosion waste acceptance criteria, [7] and ionic strength. Initial examination of blending along with the results from Task 1.1 allow for a starting point for SWPF waste acceptance criteria. [8]

WORK ACCOMPLISHED

Task 1.1

Work on the CSSX Parsons samples analyses continued to include the final sample- HB-X-X-025 (an emulsion) and results are presented. These results will also be included in a final letter report. The sample, when received, contained three distinct layers; an organic layer, a solid/emulsion layer, and an aqueous layer. The sample was thoroughly mixed and 3-1mL aliquots were removed for centrifugation and mass weights and another 5mL aliquot was removed in order to obtain a large enough sample for solids analysis. The 1-mL samples averaged an emulsion density of 0.975g/mL whereas the 5 mL sample measured 0.864g/mL at ambient temperatures. Methylene chloride was added to the 5 mL sample, thoroughly mixed, then allowed to gravity separate. The organic layer remained above the emulsion/liquid layers and was transferred via syringe to another vial for mass spectroscopy (MS) analysis. The emulsion layer appeared gel-like in consistency. The remaining aqueous portion (0.9966 g/mL) was diluted with deionized (DI) water and analyzed via ICP. The sample appears to be primarily sodium salts with sodium silicate and some gibbsite. The solids were allowed to dry for several days but retained an oily texture and no XRD analyses could be obtained until further organic removal could be performed. PLM imaging of the solids demonstrated some crystalline structure. Results from the ICP analyses are given in Table-1 while Figure-1 is the spectra obtained from MS on the organic sample. The large peak at the right is the Methylene chloride extraction solvent while the peaks on the left are associated with CSSX solvents. Evaluation of the percentage of each solvent contained in the emulsion is in progress. Figure-2 is the PLM image of the emulsion solids.

Table 1. ICP results (µg/mL) from aqueous layer of HBXX025.

Al	Na	Si	S
2.73	1079	23.0	8.6

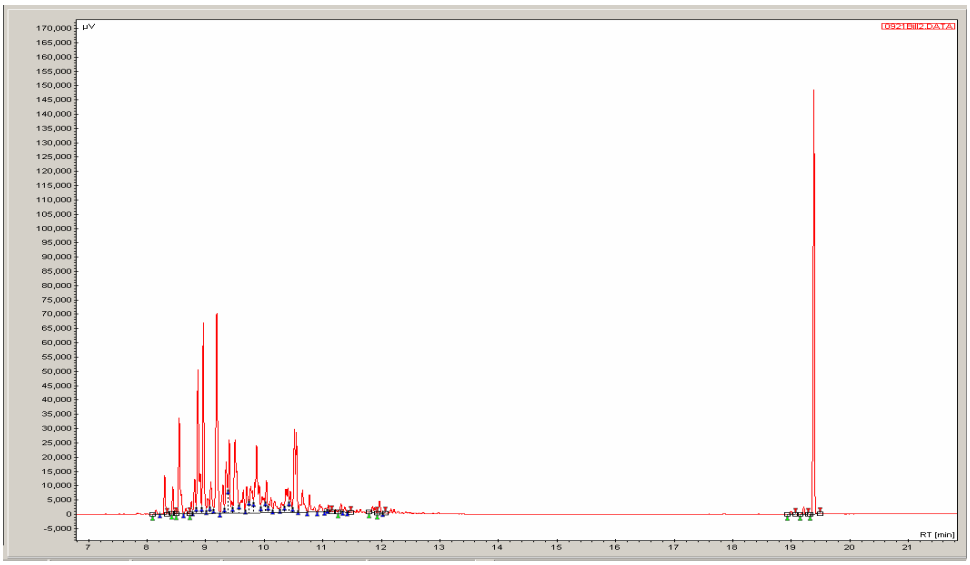

Figure-1. Mass spectroscopy spectra of organic layer in methylene chloride.

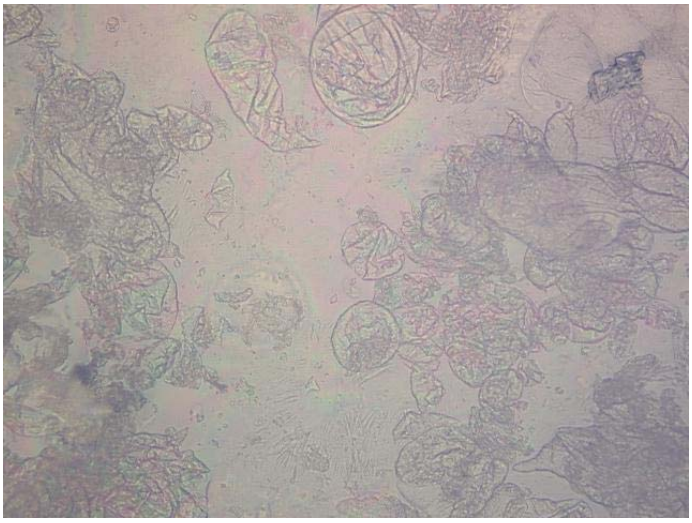

Figure-2. PLM image of crystals found in emulsion layer.

Task 1.2

Previous reports in this series have focused on the processing of waste contained within SRS tank 25F [9-11]. These calculations included the dissolution of the salt cake using the DWPF recycle stream and the subsequent processing of the stream, if necessary, to achieve corrosion protection. In this later case, the supernatant from the leaching of DWPF batch 5 can be used to adjust the hydroxide loading. Streams from later portions of the dissolution process were found to require larger additions to impart corrosion protection. Following these operations, all of the SRS waste streams will be routed to the Salt Waste Processing Facility (SWPF). One of the unit operations within the SWPF is the caustic side solvent extraction (CSSX). Here a liquid-liquid

extraction process is used to remove Cs-137 from the waste. With a lower activity, the resulting stream can be processed as saltstone while the Cs-137 rich stream will be routed to the DWPF.

Dilute nitric acid (0.05M) is used within the CSSX to scrub unbound inorganics and water from the organic extractent mixture. Small portions of the aqueous feed can encounter the acid and result in contactor fouling or solids precipitation. Recent work at Parsons Engineering has focused on the interaction of the waste stream with the acid [12]. ESP calculations have been performed in an attempt to compare to these experiments and to previous experiments conducted at General Atomics [12].

The composition of the simulant used for both series of tests is given in Table-2 [13].

Table 2 . Composition (mol/L) of the SRS simulant employed in the Parsons Testing

H_2O	4.64E+01
KNO_3	1.50E-02
CsCl	1.43E-04
NaOH	3.19E+00
$NaNO_3$	1.17E+00
$NaNO_2$	5.00E-01
$Al(NO_3)_3{\cdot}9H_2O$	2.80E-01
Na_2CO_3	1.75E-01
Na_2SO_4	1.40E-01
NaCl	2.40E-02
NaF	2.80E-02
$Na_2HPO_4{\cdot}7H_2O$	7.00E-03
$Na_2C_2O_4$	2.00E-02
Na_2SiO_3	6.98E-02
Na_2MoO_4	8.26E-05
NH_4NO_3	9.99E-04

Two flowsheets were employed for the simulations. Figure-3 accounts for the initial precipitation of solids following the preparation of the simulant and an aging period. Flowsheet 2 (not shown) considered the entire simulant to see if solids specification would be significantly different. The processes in Figure-3 are more likely to occur within the CSSX process, as it is believed that attempts to limit solids re-precipitation will be made.

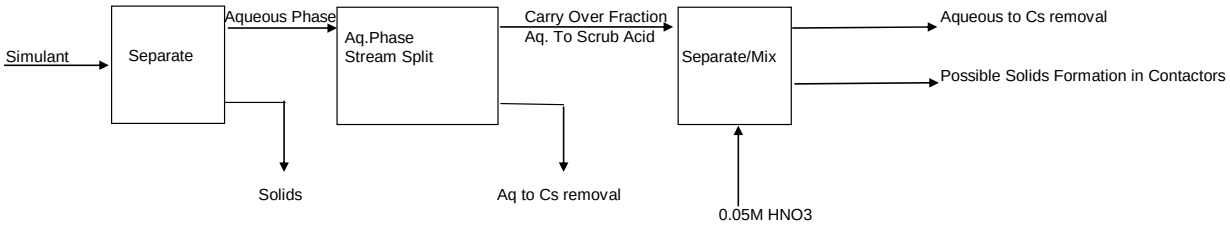

Figure-3. ESP flowsheet for mixing of the 0.05M HNO3 scrub solution with a portion of the aqueous phase of the simulant.

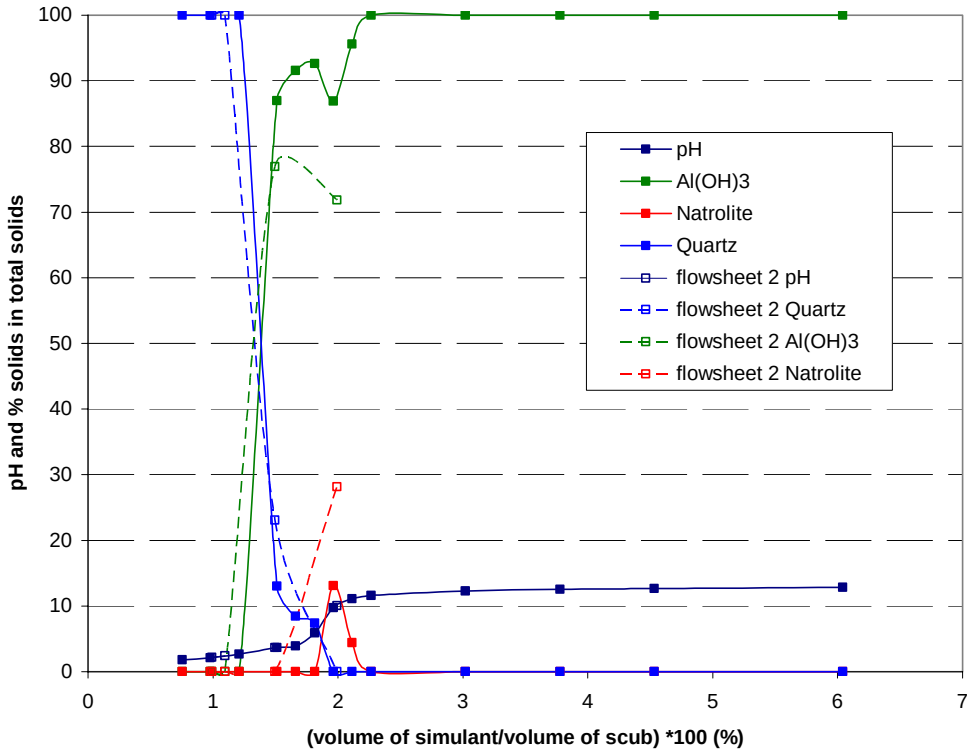

Figure-4 Effect of simulant carry-over in the 0.05M HNO_3 scrub solution.

Model results for the simulations are given in Figure-4. At low percentage carry-over, the predominant solid predicted to form is quartz, SiO_2. At still larger carry over the quartz dissolves and formation of gibbsite is expected. At around 2% simulant to 0.05 M HNO3, the solid natrolite ($Na_2Al_2Si_3O_{10}{\cdot}2H_2O$) is predicted. The potential formation within the contactors of this or other sodium aluminosilicate solids may well be problematic. Previous results on the analysis of solids from pilot-scale testing at Barnwell (Task 1.1) indicated the presence of cancrinite and other NAS solids [10, 11]. The natrolite is predicted to form between a pH of around 9.7 -11.2. Correlation of the xrd results from work in these laboratories with the various contactor stages (extraction, scrub, and strip) is in progress.

Similar results are observed for the modified flow sheet where the same solids are predicted to form in similar pH ranges, Figure-4.

Additional ESP simulations were carried out for comparisons to pH measurements at Parsons [12]. Comparisons of the ESP model predictions with the pH values measured for three different runs are given in Figure-5. Good agreements between the model predictions and the measured pH values are observed at low percentage carry-over. As the carry-over becomes larger, there seems a shift in the pH values predicted by the model. The general shapes of the curves, including the inflection point around pH of 4 are similar. Discrepancies between the measured and calculated values may arise from temperature differences. A temperature of 23°C was assumed in the ESP calculations.

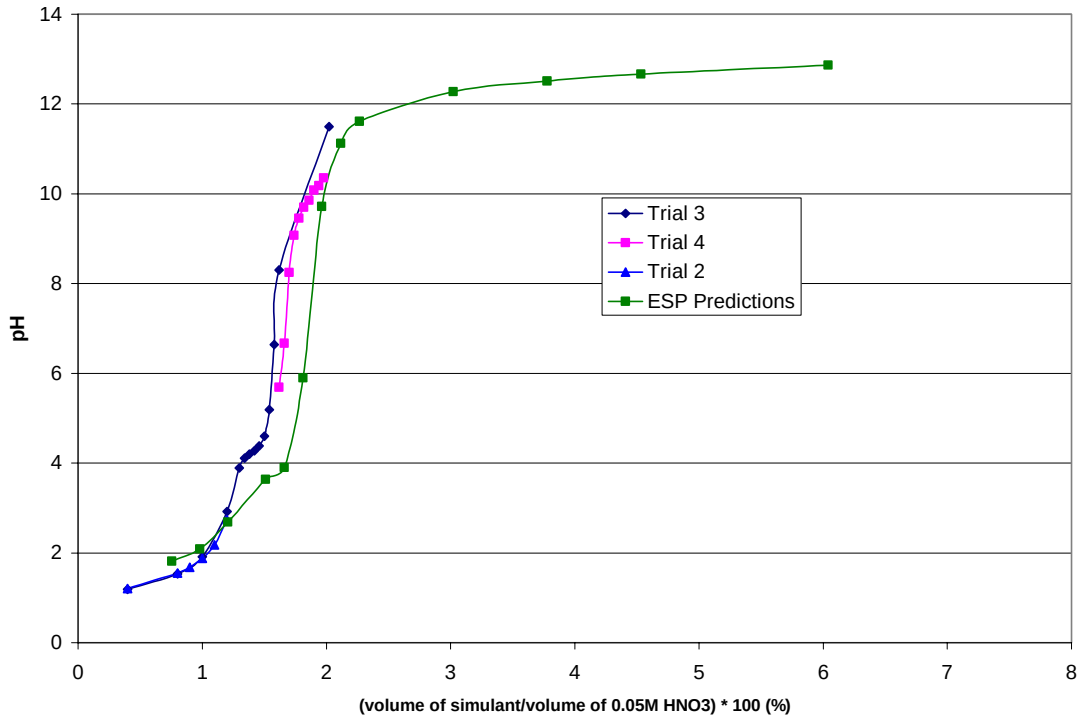

Figure-5. Comparison of ESP pH predictions, Figure-4, with measured pH values (meter and indicator paper).

The impacts of aqueous phase carry over to the nitric acid scrub were then evaluated for some of the transfer streams arising from the processing of Tank 25F. For these calculations the aqueous phases was separated from the solids (see reference 11) and then a small fraction of the waste stream was mixed with the acid. The simulation temperature was set at 23^{o}C. Figure-5 shows the change in pH as a function of the aqueous phase carry over for transfer stream 1, 4, and 6.

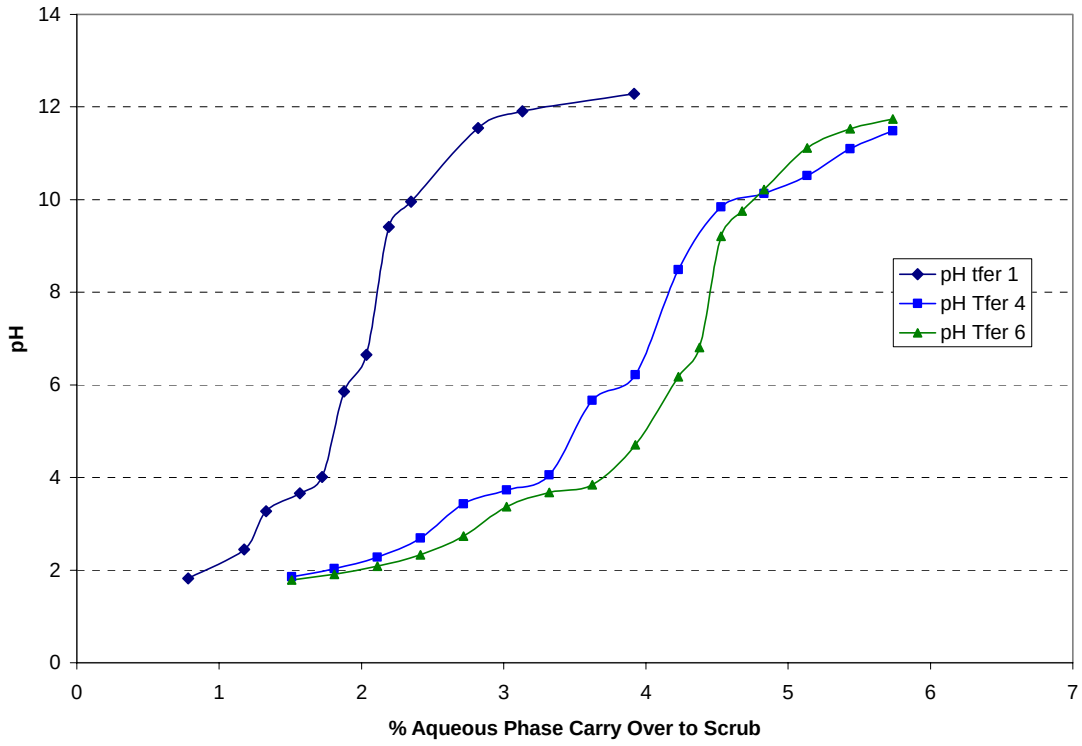

Figure-6. Variation of the pH as a function of carry over for three streams originating at different dissolution stages from SRS Tank 25F.

The data is similar to that obtained by Brugh, Figure-5 [12]. There is an initial gradual increase in pH followed by a region where the pH is not significantly increasing, followed again by a strong increase. At larger percentages of carry over the pH begins to approach an asymptotic range that would eventually coincide with the pH of the original waste stream.

Changes in the pH (carry over) result in changes in the solid-liquid equilibrium. A number of different solids were predicted including, $Al(OH)_3$, Cr_2O_3, Fe_2O_3, $Mn(OH)_2$, $Ni(OH)_2$, Dawsonite, ($NaAlCO_3(OH)_2$), $TcO_2 \cdot 2H_2O$, and UO_2. The major solid formed was Gibbsite, followed by Dawsonite, and at pH values greater than 11, $Mn(OH)_2$. Table-3 provides the resulting solids distribution as a function of pH for selected simulations concerning transfer stream 4. While these solids loadings may appear large, it is important to note that anywhere from 2.49×10^6 to 9.46×10^6 g of waste supernatant was added to 1.22×10^8 g of the 0.05M HNO_3 scrub solution. Consequently, the overall percentage solids formation at the different carry over or pH values was less than 0.07 (by weight) for the three streams investigated, Figure-7.

Table-3. Solids distribution and loading (g) for some of the simulations associated with the carry over of 25F transfer stream 4 to the CSSX scrub solution.

pH	1.86	2.03	5.67	8.49	9.84	10.13	10.51
% carry over	1.51	1.81	3.62	4.23	4.53	4.83	5.13
Solids Predicted (g)							
$Al(OH)_3$			3.2E+04		5.5E+03	3.3E+04	4.5E+04
$NaAlCO_3(OH)_2$				6.9E+04	6.3E+04	1.8E+04	
$Mn(OH)_2$							
Cr_2O_3				1.0E-03	1.1E-03	1.1E-03	1.2E-03
Fe_2O_3				4.3E-02	4.6E-02	4.9E-02	5.2E-02
$Ni(OH)_2$							4.5E-01
$TcO_2 \cdot 2H_2O$				3.5E-01	3.8E-01	4.0E-01	3.9E-01
UO_2		2.4E-01	7.5E-01	8.8E-01	9.4E-01	9.9E-01	1.0E+00

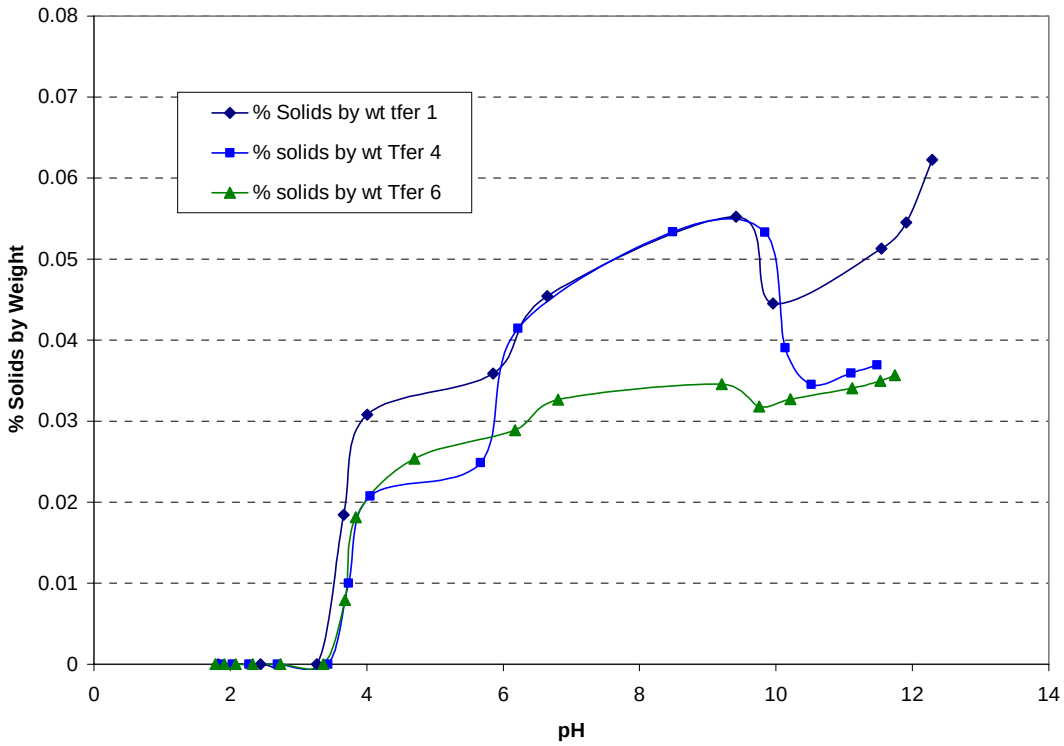

Figure-7. The effect of pH from mixing the aqueous phase transfer streams with the nitric acid scrub solution on the resulting total solids loading.

An interesting prediction from the calculations concerns the partitioning of Gibbsite and Dawsonite, Figure-8. The ESP simulation predicted that at low carry over values (low pH) the predominant solid formed is Gibbsite. As the pH increase to the range of around 6-10 the predominant solid becomes Dawsonite; at still higher pH Gibbsite again dominates. This result

is similar to the competition between Gibbsite and Natrolite formation of the base SRS simulant used by Parsons, Figure-3 and Table-2). Further experimentation is needed to fully evaluate these transitions and simulant compositions based on the transfer streams are under development.

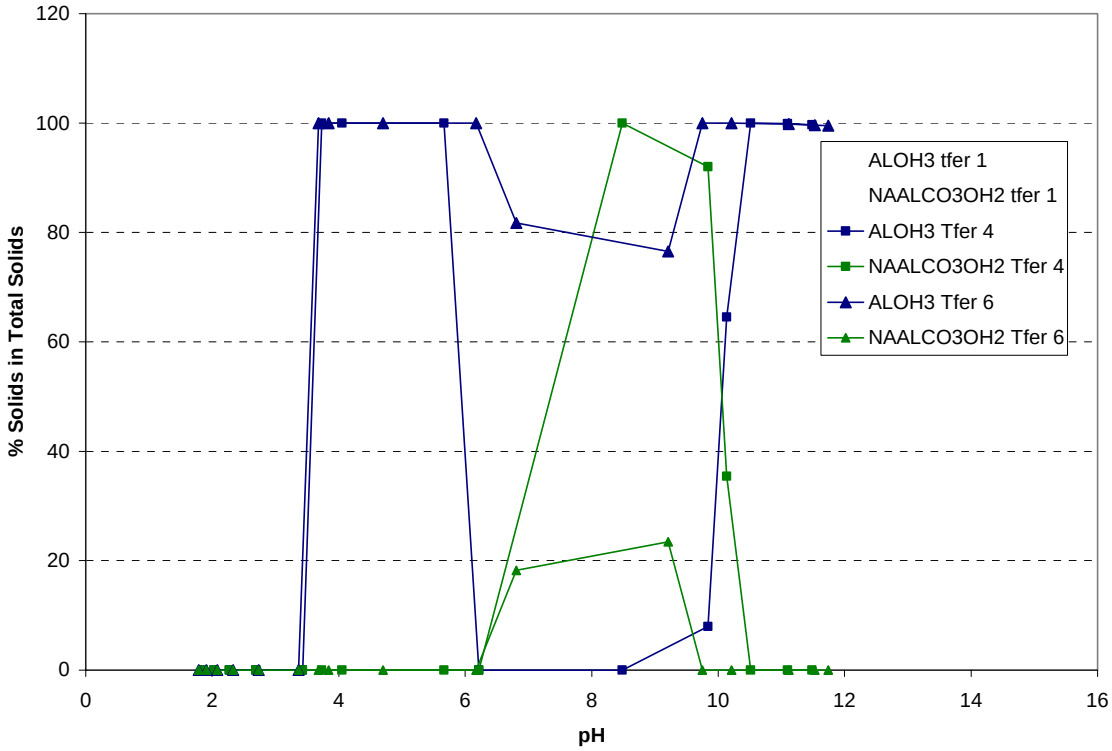

Figure-8. Variation of the main solids predicted by the simulations (Gibbsite and Dawsonite) as a function of pH.

CONCLUSIONS

Analysis of the seven samples sent from Parsons on the CSSX simulant tests is now complete. All results will be included in a final letter report sent to site personnel.

Extensive ESP simulations are reported on recent CSSX tests performed at Parsons Engineering and on expected waste compositions from dissolution of SRS Tank 25F. General trends in the pH values measured at Parsons on adding aqueous phase simulant supernatant to the 0.05M HNO_3 scrub solution in the CSSX process, and the predicted values were observed. Model results also indicated the partitioning of Gibbsite and Natrolite. Further comparisons will be possible on additional sample analysis. Evaluations of three of the dissolution or transfer streams from 25F indicated that the primary solids that undergo re-precipitation on carry over of the waste stream to the scrub solution were Gibbsite and Dawsonite. Trends in the pH with carry over were similar to those observed at Parsons but were shifted owing to changes in the feed composition. Overall, the resulting solids loading remained below 0.07% by weight indicating that minimal fouling would be expected. Further work is in progress to address simulant development and testing to fully characterize the potential impacts on solids formation within the CSSX contactors.

WORK FORECAST

Modeling of the CSSX simulants and the areas where emulsion formation may occur will continue. Analyses will be performed as additional samples are received.

All of the simulations associated with the retrieval of SRS tank 25F and the subsequent processing of the waste using the DWPF recycle stream, water, and the supernatant from the Batch 5 leachate will be compiled for presentation at the next Information Exchange, tentatively scheduled for late Spring in Hanford. The results described in this report will also be included. Work will commence on the retrieval and processing of wastes contained in SRS tanks 31, 37, and 38H, simulant development from one or two 25F transfer streams and laboratory experiments simulating carry over into the CSSX scrub solution.

REFERENCES

1. Dimenna, R.A.; Elder, H.H.; Foweler, J.R.; Fowler, R.C.; Gregory, M.V.; Hang, T.; Jacobs, R.A.; Paul, R.K.; Pike, J.A.; Rutland, P.L.; Smith, F.G.; Subosits, S.G.; Taylor, G.A.; Campbell, S.G.; Washburn, F.A. "Bases, Assumptions, and Results of the Flowsheet Calculations for the Decision Phase Salt Disposition Alternatives" WSRC-RP-99-00006, Rev. 3, Westinghouse Savannah River Company, Aiken, SC (2001).
2. Leonard, R.A.; Aase, S.B.; Arafat, H.; Conner, A.C.; Chamberlain, D.B.; Falkenberg, J.R.; Regalbutto, M.C.; Vandergrift, G.F. "Experimental Verification of Caustic-Side Solvent Extraction for Removal of Cesium from Tank Waste" *Sol. Extr. and Ion Exch.* **21(4)**, *2003*, 505.
3. Campbell, S.G.; Geeting, M.W.; Kennell, C.W.; Law, J.D.; Leonard, R.A.; Walker, D.D. "Demonstration of Caustic-Side Solvent Extraction with Savannah River Site High Level Waste" WSRC-TR-2001-00223, Rev.1, Westinghouse Savannah River Company, Aiken, SC (2001).
4. Weber, E.J. "Aluminum Hydroxide Dissolution in Synthetic Sludges" DP-1617, 1982.
5. Hay, M.S.; Pareizs, J.M.; Bannochie, C.J.; Stone, M.E.; Click, D.R.; McCabe, D.J. "Preliminary Data from the 3L Tank 51H Aluminum Dissolution Test" SRNL-CST-2007-00102, Savannah River National Lab, Aiken, SC (2007)
6. Ketusky, E., "High Level Waste System Impacts from Acid Dissolution of Sludge" CBU-PIT-2005-00260R1, Westinghouse Savannah River Company, Aiken, SC (2005).
7. Fox, L., "CSTF Corrosion Control Program," WSRC-TR2002-00327, Rev. 3, Westinghouse Savannah River Company, Aiken, SC (2003).
8. Waste Acceptance Criteria for Aqueous Waste sent to the Z-Area Saltstone Production Facility (U). X-SD-Z-00001, Rev. 2, 2004.
9.. Lindner, J. S. and L. T. Smith, "Modeling and Experimental Support for High Level SRS Salt Disposition Alternatives," in Accelerating Cleanup of the Defense Nuclear Legacy, Report No.07040R02, Institute for Clean Energy Technology, Mississippi State University, 2008, JFM report please check

10 Lindner, J. S. and L. T. Smith, “Modeling and Experimental Support for High Level SRS Salt Disposition Alternatives,” in Accelerating Cleanup of the Defense Nuclear Legacy, Report No.07040R02, Institute for Clean Energy Technology, Mississippi State University, 2008, AMJ report, please check
11. Lindner, J. S. and L. T. Smith, “Modeling and Experimental Support for High Level SRS Salt Disposition Alternatives,” in Accelerating Cleanup of the Defense Nuclear Legacy, Report No.07040R02, Institute for Clean Energy Technology, Mississippi State University, 2008, JAS report please check
12. Brugh, Mark, personal communication, fall 2008.
13. Fahr, A, Basset, M. and M. Brugh, "Milestone Progress Report for CSSX Dispersion (Emulsion) Task," May 5, 2008 Parsons Engineering, Aiken SC, pg 6

Task 2

Process Improvements for the Defense Processing Facility (DWPF)

Jagdish P. Singh

INTRODUCTION

An on-line, real-time analysis of Defense Waste Processing Facility **(**DWPF) samples will significantly increase analytical throughput and will reduce waste generation in radiological analytical facilities. The goal of this Task is to develop system for rapid analysis of DWPF samples to accelerate waste processing using laser-induced breakdown spectroscopy (LIBS).
The first subtask of this project will provide a system for direct analysis of slurry in the DWPF's analytical shielded cells. The capability of direct analysis of slurry will significantly increase analytical throughput and will reduce waste generation in radiological analytical facilities, providing analyses suitable for waste acceptance and production records. The second subtask is to provide compositional data for plutonium residue feeds before being processed into glass.
LIBS uses a high pulse energy laser beam to produces a micro plasma to vaporize, dissociate, excite, or ionize species on material surfaces. The study of the atomic emission from the micro plasma provides information about the composition of the material. LIBS is a powerful analytical tool which is suitable for quick and on-line elemental analysis of any phase of material.[1-4] The laser light and emitted signal can be delivered via optical fiber so it is useful for hazardous situations. LIBS can provide an accuracy of 3-5% for elements with concentration >1% and an accuracy of 5-10% or better for minor elements in solid samples.

WORK PERFORMED

LIBS experiments of DWPF slurry continued. One problem we observed early with the direct sampling slurry in a beaker is slurry sedimentation. The slurry sample need to be continuously stirred by magnetic stirrer during the LIBS measurement. If the stirring speed is not fast enough the sedimentation problem still exist and the measurement on the surface cannot represent the bulk. However, if the stirring rate is too fast, the sample surface is seriously disturbed and results the sample to surface distance variation and poor measurement reproducibility. To find the solution for the direct sampling, we have evaluated a sampling method that uses a substrate to hold small amount of slurry samples for LIBS measurement. Figure 1 shows the experimental setup used to record LIBS spectra of DWPF slurry on a substrate. A frequency-doubled, Q-switched Nd:YAG laser (532-nm) is focused onto a thin layer slurry sample on substrate using an ultraviolet grade quartz lens of 300 mm focal length. Atomic

emission from the laser-induced plasma was collected by an optical fiber bundle using a UV-grade quartz lens and sent to an Echelle spectrograph (ESA 3000, LLA Instruments, GmbH, Germany) with 1024×1024 element intensified charge coupled device. The substrate was placed on a rotating stage, which will rotate during LIBS measurement to make sure a new spot was sampling for each laser shot. In our initial investigation, we used 2" diameter filter paper as substrate. A thin layer of slurry was coated on the filter paper and let dry for 20 minutes before LIBS measurement. Figure 9 show some preliminary results obtained from these measurements. Those data were taken in a period of 20 minutes. The LIBS signal ratios shows an improved relative standard deviation (RSD) ~4-8% as compared to RSD about 10-20% from direct sampling slurry from a beaker. The preliminary results are encouraging, more tests with filter paper and other types of substrates will need to be conducted to find the best substrate for slurry measurement. During one of the slurry experiments the water tube coupling nipple on the Echelle Spectrometer ESA3000 end was broken. Due to the delicate design of the spectrometer, it require technical expert from manufacturer to replace the water connectors inside the spectrometer. The manufacturer currently does not have any representative in US, we have to send the whole detection system to Germany for repair and re-calibration. The slurry measurement will be resumed after this spectrometer is fixed.

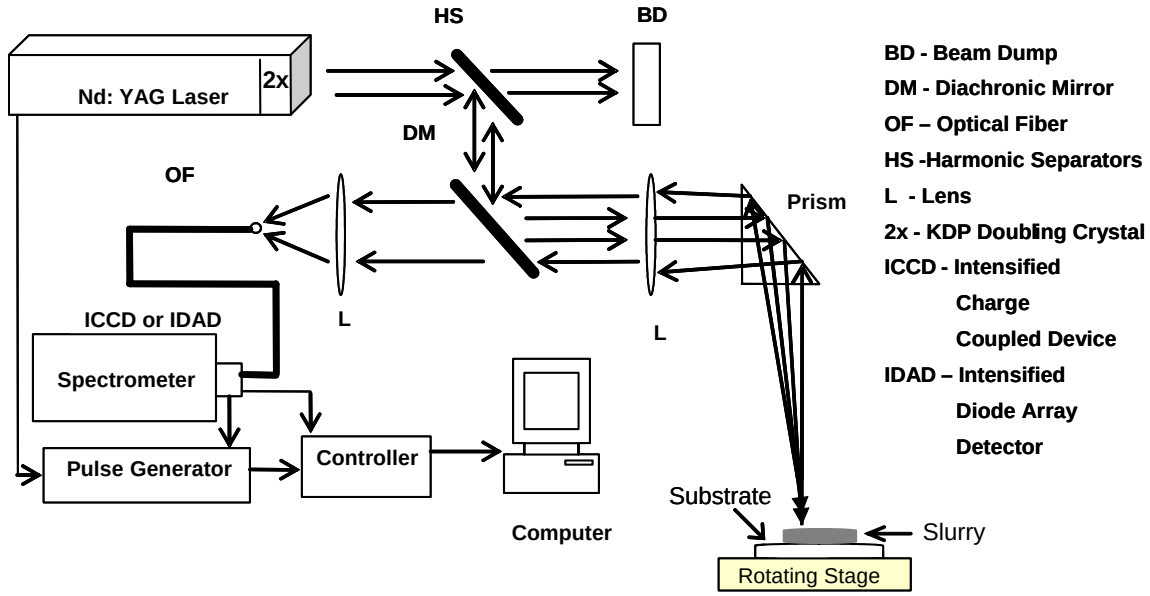

Figure 9. LIBS experimental setup for slurry sampling on substrate.

A compact broadband spectrometer (Mechelle 5000, Andor Techholoy) purchased for a fieldable LIBS system was integrated with the double pulse (DP) laser system (Big Sky Laser CFR PIV-200). This broadband spectrograph can provide simultaneous recording of a wide wavelength range (200-975 nm) in one acquisition. It has built-in Digital Delay Generator (DDG) for precise gate control. The compact and robust design of this spectrometer is ideal for field measurement**.** The schematic of this fieldable LIBS system is shown in Figure 10. Initially, the whole system is being tested with several solid samples. First, we tested this system with the

sample contains only few elements to obtain the best experimental setup with this system.

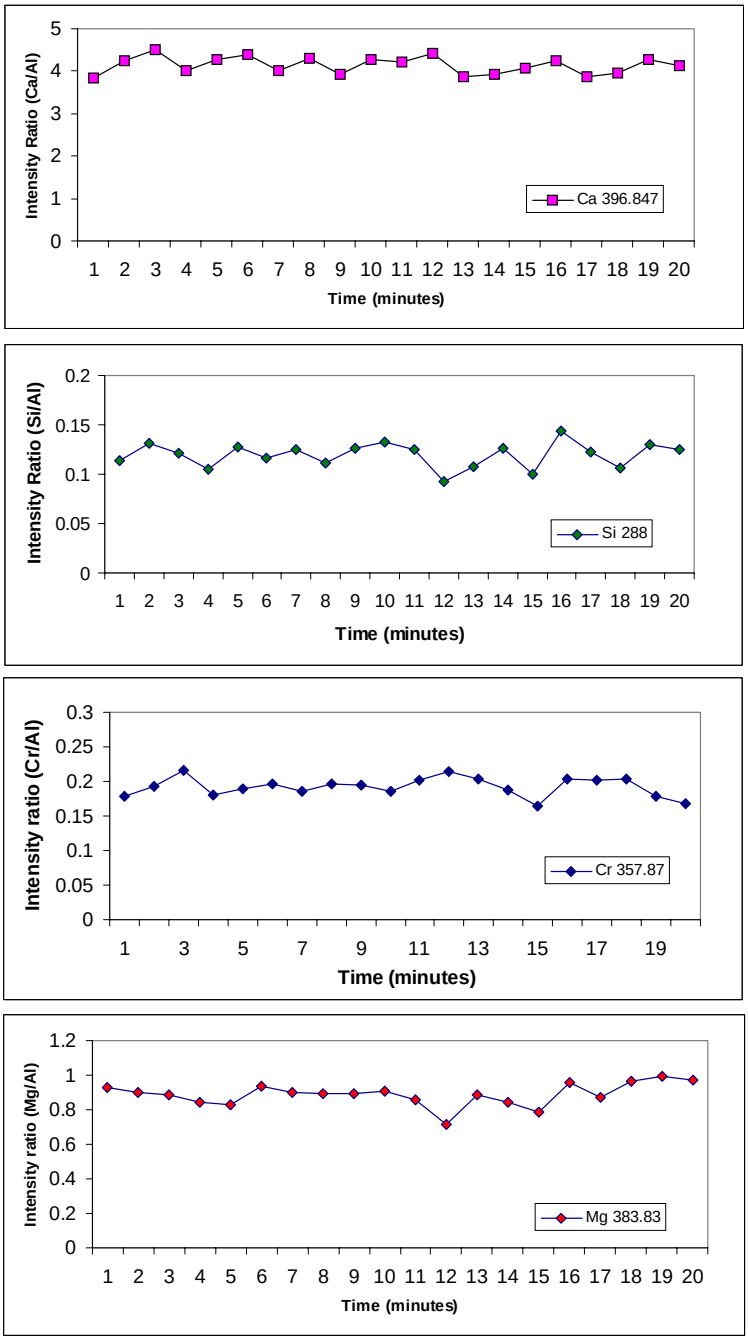

Figure 10. LIBS signal variation with time. The data were obtained from slurry on a filter paper.

Then, data was collected with a more complicated matrix sample to study the spectral interference problem with this detection system. This LIBS system can operate in either single pulse or double pulse mode depending on the application requirement. We have collected some

DP- LIBS data of aluminum alloy with the DP laser system and a Czerny-Turner spectrometer earlier.[5] To evaluate the performance of this compact broadband spectrometer, we have recorded some DP-LIBS data of aluminum alloy. Figure 11 shows the intensity variation of three Mg lines at different interpulse delay recorded with the fieldable LIBS system. It shows that the peak intensity of atomic emission lines gradually increases up to certain inter-pulse delay then it starts decreasing. It shows that at certain delay the optimum condition can be achieved when second pulse will interact with plume generated by first pulse to obtain the maximum enhancement.

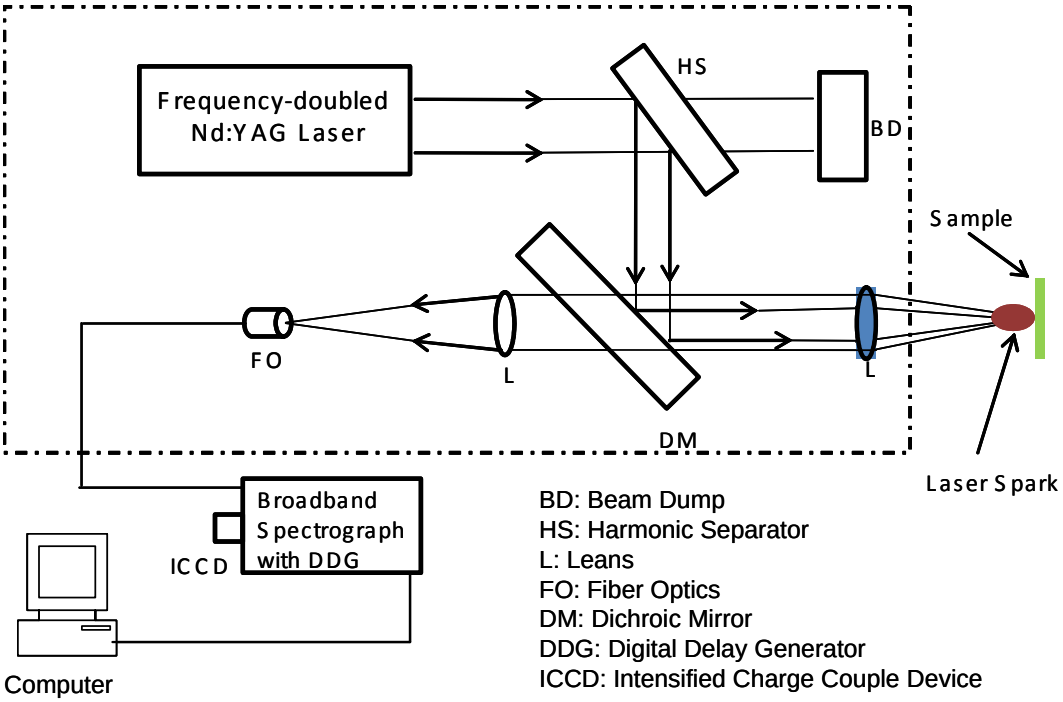

Figure 11. Double-pulse LIBS experimental setup using a compact broadband spectrometer.

The similar data recorded with a Czerny-Turner spectrometer is given in Figure 12a for comparison. The intensity variation pattern from these two detection systems is similar for interpulse delay greater than 5 μs. The difference in signal enhancement between these two detection systems observed below 5μs is believed to be due to small difference on experimental alignment. We have also tested the fieldable system for recording plutonium surrogate pellet data. The composition of pellet sample is given in Table 4.

Figure 12b shows part of the DP-LIBS spectrum of pellet recorded at different interpulse delay. It shows that using double pulse LIBS significant enhancement for the Cr, Ce, Mo, and Gd lines was observed at an interpulse delay near 2μs. These preliminary test results shows that improved LIBS limit of detection can be achieved with this fieldable LIBS system operated under an optimum interpulse delay for that sample.

.

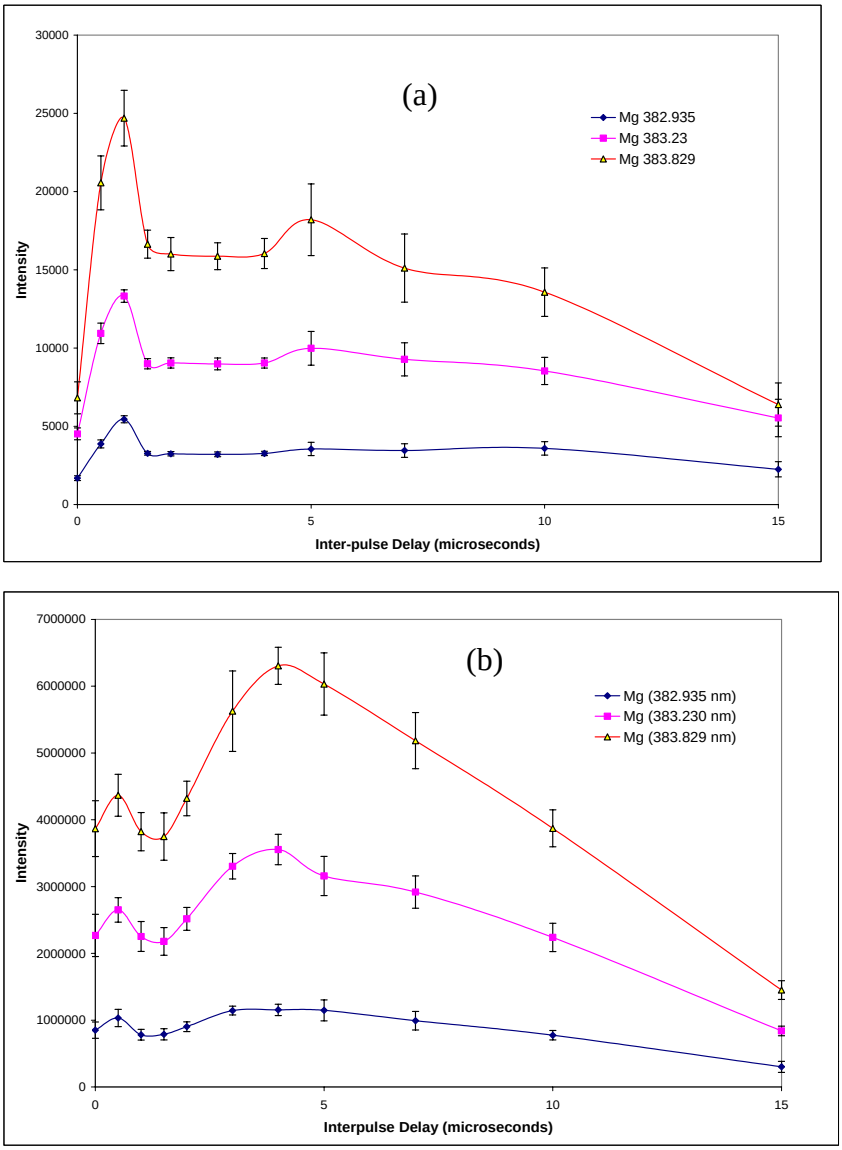

Figure 12. Intensity variation of Mg lines at various interpulse delay in DP- LIBS of Al Sample with a) broadband Mechelle 5000 spectrometer and b) Czerny-Turner spectrometer.

Table 4. The composition of the CeO2-batch pellet used in the test

Compound	Wt%	Compound	Wt%
Cr_2O_3	6.08	NiO	0.72
MoO_3	5.72	ZnO	0.18
WO_3	2.16	Al_2O_3	6.62
SiO_2	1.44	Gd_2O_3	2.97
Ta_2O_5	14.40	MgO	2.88
Fe_2O_3	1.67	CeO_2	55.00

Work Forecast

Software for the fieldable LIBS system will be developed to allow on-line, real-time data acquisition and analysis. Work to improve the performance of slurry measurement with different sampling methods and data processing techniques will continue.

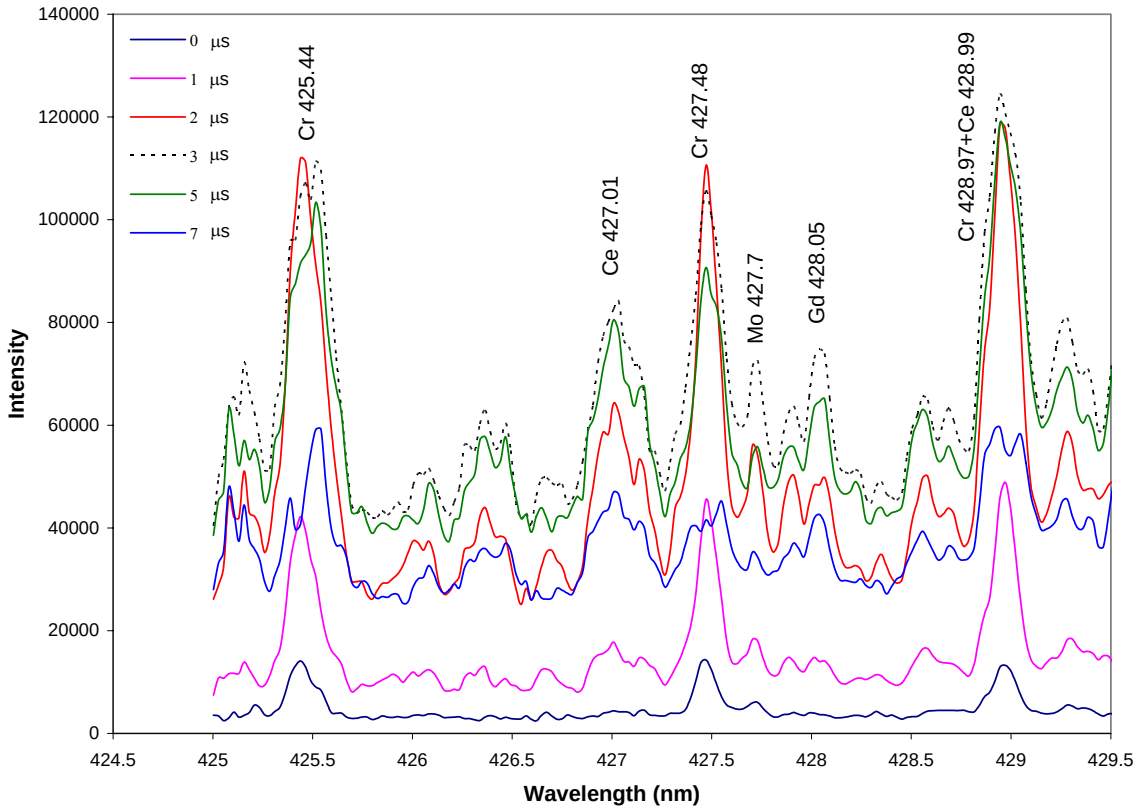

Figure 13. Part of a double pulse LIBS spectra from 55% CeO2 –batch pellet recorded at different inter-pulse delay times

Conclusion

A compact spectrometer and a double-pulse laser system were integrated as a fieldable LIBS system. This system is compact, sturdy, and easy to realign. The performance of this LIBS system is being evaluated with some solid samples. It can perform single pulse LIBS and double-pulse LIBS measurement depending on the application. Its broad spectral coverage allows the detection of all the elements simultaneously. A data analysis program needs to be developed for this system to process large amount of data recorded with this system. In order to improve the performance of slurry sampling, we have tested the methods that using substrates to hold small amount of slurry for LIBS measurement and obtained some promising initial results.

References

1. J. P. Singh and S. N. Thakur, Laser- Induced Breakdown Spectroscopy, Elesvier Science B. V., Amsterdam, The Netherlands, 2007.
2. A. Miziolek, V. Palleschi and I. Schechter, Laser- Induced Breakdown Spectroscopy (LIBS): Fundamentals and Applications, Cambridge University Press, 2006.
3. Fang-Yu Yueh, Jagdish P. Singh and Hansheng Zhang, "Laser-induced breakdown spectroscopy-elemental analysis", in *Encyclopedia of Analytical Chemistry*, R.A.Meyers, ed. (Wiley, New York, 2000).
4. Celio Pasquini; Juliana Cortez; Lucas M. C. Silva; Fabiano B. Gonzaga "Laser Induced Breakdown Spectroscopy, J. Braz. Chem. Soc. 18(3), 463 (2007).
5. Technical Progress Report 07040R03, July 1, 2008 - September 30, 2008, DOE Agreement No. DE-FC01-06EW-07040.

Task 3

High Efficiency Particulate Air (HEPA)

Rangaswami Arunkumar, Charles A. Waggoner

Activities associated with autopsying loaded filters to evaluate patterns of buildup on the surface of filter media as a function of aerosol challenge will be completed during the 4th quarter of 2008. A test plan will be developed for the process of evaluating excursions below safety design basis. A new series of investigations will be planned to identify the range of upset conditions encountered by HEPA filters that would not automatically result in their replacement. Additional efforts will be made to identify alternate funding sources for continuation of ICET's HEPA filter research program.

Task 4

Support of Hanford Single Shell Tank Waste Disposition

Jeffrey Lindner, John Luthe, Larry Pearson, Laura Smith, Rebecca Toghiani

INTRODUCTION

Knowledge of the chemistry associated with the wastes contained in the Hanford tank farms has bearings on waste pretreatment, retrieval, vitrification, alternative processing, and tank closure operations. Much of the work conducted at ICET has focused on developing an understanding of the salt chemistry found in these tanks. A number of experiments have been performed and have led to the development of the V7DBLSLT thermodynamic database for use in the OLI Systems Inc. Environmental Simulation Program (ESP). This work consisted of extensive solubility measurements of specific sodium salt systems at the temperatures and pH values typical of the site waste [1,2]. Additional efforts were directed at aluminum chemistry and with development of a neural network model based on a framework of ESP simulations for use in conjunction with the Hanford H2 (overall campaign flowsheeting) simulator.

The Hanford Tank Waste Operations Simulator (HTWOS) is used for scheduling the entire retrieval campaign and includes model representations for vitrification and low activity waste processes. Chemistry representations used in HTWOS rely on wash and leach factors as opposed to direct, solid-liquid equilibrium thermodynamic calculations. Site engineers have previously requested an evaluation of the feasibility of upgrading the chemistry representation to include ESP. Having a proper chemistry representation within HTWOS will reduce the uncertainties associated with wash and leach factors. Earlier work identified the use of a neural network as a preferred option due to the large number of calculations needed during a HTWOS campaign run. As an initial evaluation of this approach, site engineers requested the application of the process to the retrieval of C farm tanks.

The development of a neural network for use within the HTWOS model requires an extensive set of training data. To generate this data, ICET constructed an ESP program process model of the retrieval of C tank waste based on the procedures and constraints followed in the Modified Sluicing Method [3] of waste retrieval. With this ESP simulation framework, a neural network training set consisting of the input stream values and the ESP computation output can be built.

Construction of the training set to cover the ranges of possible input streams requires an execution of the ESP program for each case. Since ESP is an interactive program, a batch mode processing routine is necessary to replace the ESP user interface. Perl [4], a freely available platform independent programming language was used to provide this batch mode processing. The retrieval of C-108 waste using flush liquid from AN-106 was simulated with the ESP program process model and Perl to provide the initial neural net training data. Simulations of each of the remaining C farm tanks, using this model, will provide the data necessary for the generation of an expanded neural network training set applicable across the entire range of C farm tank compositions. This expanded neural network will allow an evaluation of the retrieval schedule including different combinations of source and destination tanks. Since the neural network utilizes equilibrium chemistry as its basis, the potential result is a more accurate, as well as, timely method for Hanford campaign simulation.

WORK ACCOMPLISHED

The retrieval of waste from the Hanford C farm tanks is currently scheduled to utilize two waste recovery techniques. The Modified Sluicing with Recycle method (MSwR) has been selected for use in the majority of tanks. This method has been modeled using the OLI ESP equilibrium program as reported previously [3,5].

AY-101

The retrieval of C farm tanks C-107, C-101, and C-105 will make use of both techniques. C-107 is scheduled for use of the MSwR method while C-101 and C-105 will be retrieved using the MRS method. The sequence of the retrievals is C-107 followed by C-101 and then C-105. The destination tank for each of these C tanks is AY-101. Modeling of each tank retrieval was performed utilizing the OLI ESP equilibrium program to be consistent with the prior MSwR and MRS simulations. The basic structure of the MSwR model was maintained as a four stage process with constraints as previously reported [3]. The MRS model consists of two stages with constraints also previously reported [5].

Table 5 displays several parameters of AY-101 during the complete retrieval of the C tanks. These same parameters for the flush stream that is returned to the AY tank are also displayed. The stage numbers correspond with each stage of the process with the initial state listed as stage 0. Figures 14 and 15 display several of these parameters in chart form. Figures 16 and 17 graphically show conditions of the flush stream that is returned to AY-101. Table 6 shows the amounts of several of the major solids which are collected and appear in AY-101. Again, these solids are shown after each stage of the total retrieval process. Figures 18 and 19 show these major solids in chart form.

Table 7 shows the conditions present in each of the C tanks during the retrieval process. Again, stage 0 is used to represent the initial conditions in the tank.

Table 5 – AY tank and flush conditions during retrieval of C-107, C-101, and C105

			C-107				C-101		C-105	
	stage	0	1	2	3	4	5	6	7	8
	gallons	831,878	836,960	1,135,762	1,147,758	1,153,042	1,171,131	1,197,600	1,276,624	1,303,775
	specific gravit	1.21	1.21	1.23	1.24	1.24	1.25	1.26	1.30	1.32
AY-101	wt% solids	8.26	8.26	15.36	16.37	16.78	17.37	18.85	21.62	23.06
Tank	vol% solids	3.73	3.73	7.46	8.01	8.23	8.64	9.56	11.25	12.11
Conditions	Na molarity	3.13	3.13	2.61	2.61	2.61	2.74	2.78	2.98	2.98
	pH	12.20	12.19	11.84	11.84	11.84	11.88	11.89	11.93	11.93
	wt% water	74.96	74.95	70.64	69.80	69.45	68.08	67.09	63.58	62.40
	stage		1	2	3	4	5	6	7	8
	gallons		5,283	1,092,432	368,635	612,876	114,301	687,830	614,556	727,211
Flush	specific gravi		1.17	1.19	1.15	1.13	1.25	1.16	1.23	1.18
Return to	wt% solids		2.44	9.99	4.21	1.09	9.91	4.18	9.91	4.17
AY-101	vol% solids		0.94	4.78	1.96	0.50	5.42	2.06	4.86	1.96
	Na molarity		3.83	2.61	2.61	2.61	3.96	2.77	3.14	2.98
	pH		7.08	11.80	11.84	11.84	12.93	12.00	12.11	11.93
	wt% water						68.03	79.34	72.10	77.71

Table 6 – AY-101 Solids during the Retrieval of C-107, C-101, and C-105

AY-101 Solids		C-107				C-101		C-105	
stage	0	1	2	3	4	5	6	7	8
Total gmoles	2,837,850	2,844,980	5,903,864	6,332,414	6,513,375	6,998,494	8,144,092	11,652,932	13,324,577
ALOH3	942,384	926,894	1,570,879	1,661,149	1,699,228	2,196,649	3,270,805	6,714,660	8,340,800
BIOH3	218	287	37,242	42,332	44,479	44,601	44,902	45,954	46,456
CROH3	40,909	41,258	54,367	56,173	56,934	57,645	59,373	63,770	65,868
FEIIIOH3	813,111	815,651	2,185,659	2,374,358	2,453,968	2,480,166	2,544,426	2,587,539	2,608,179
NIOH2	32,194	32,584	71,661	77,044	79,314	79,454	79,854	96,618	104,609
FAPATITE	7,311	7,319	11,954	12,592	12,861	14,408	18,101	23,969	26,766
NA2C2O4	255,192	254,567	198,765	198,336	198,331	202,746	207,873	209,088	209,609
NAALCO3OH2	743,328	763,164	1,741,000	1,874,088	1,930,228	1,877,655	1,856,554	1,824,560	1,823,807
UIVO2	3,203	3,256	32,337	36,343	38,033	45,170	62,205	86,773	98,483

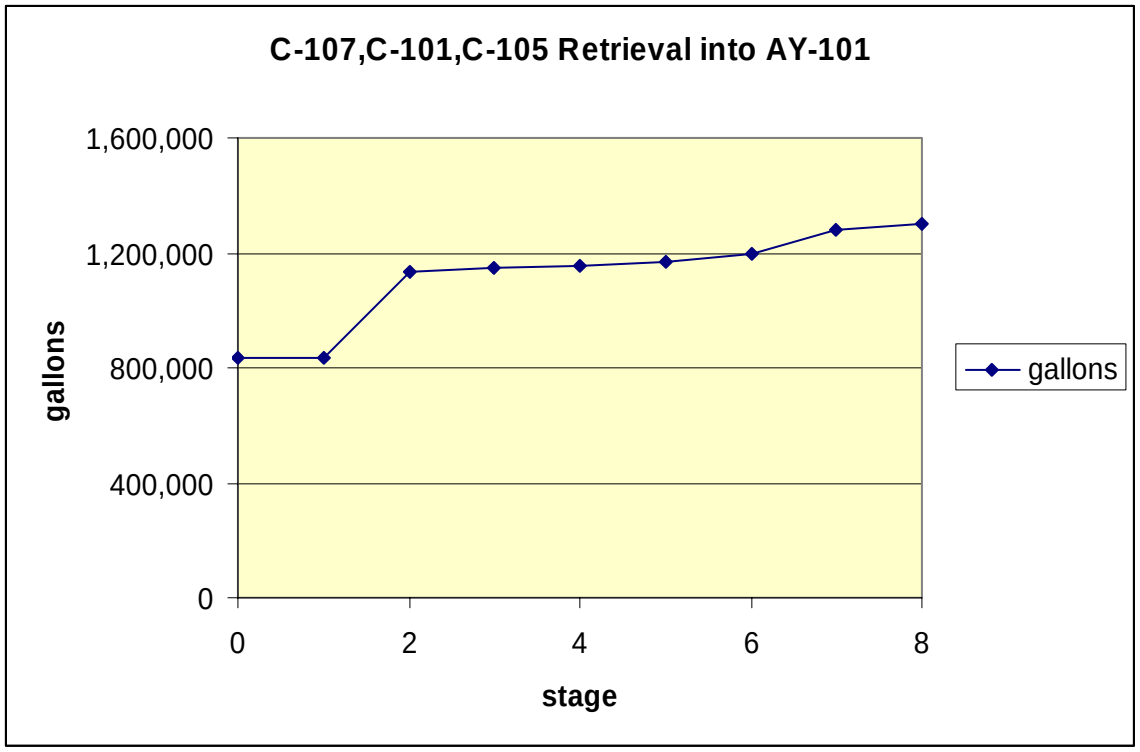

Figure 14 – Total Volume of AY-101 during retrieval of C tanks

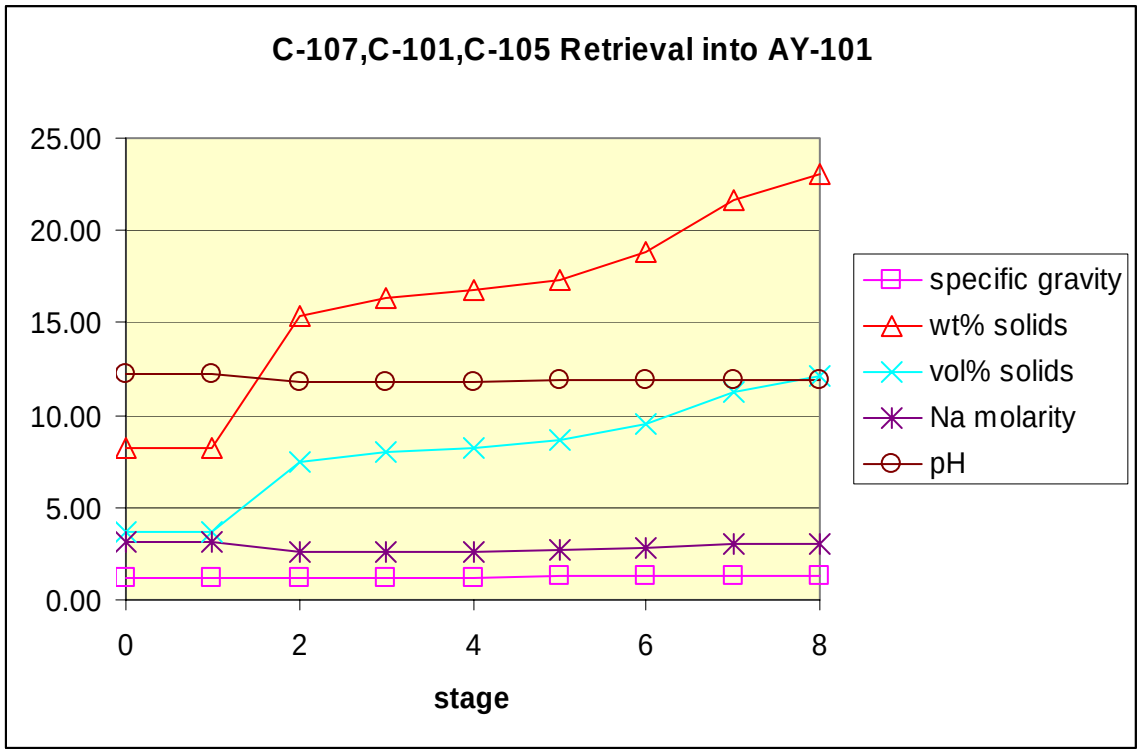

Figure 15 – AY-101 Conditions during retrieval of C tanks

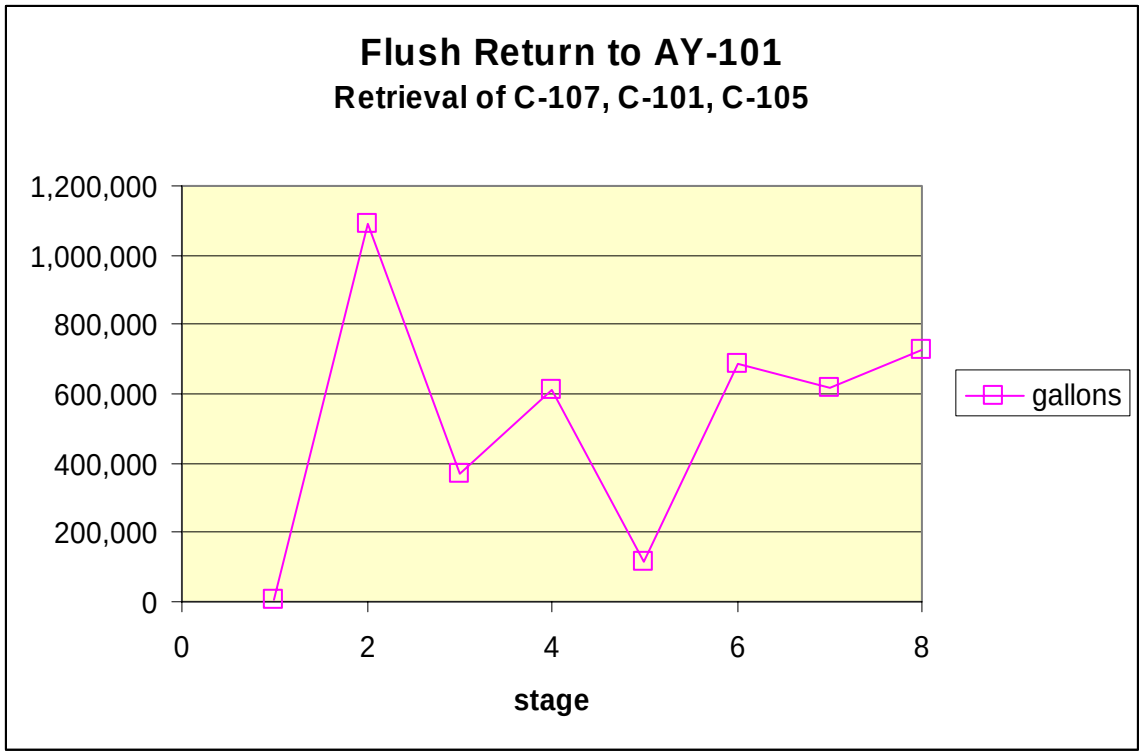

Figure 16 – Total Volume of Flush Stream to AY tank

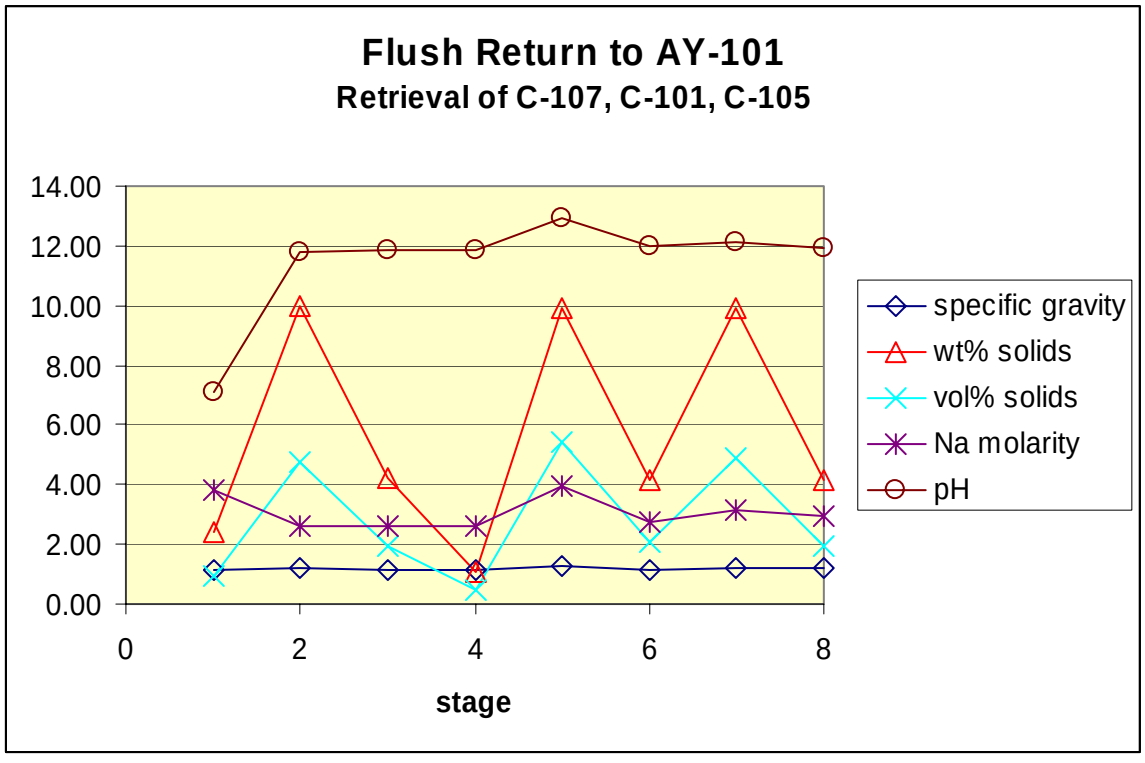

Figure 17 – Conditions of Flush Stream to AY tank

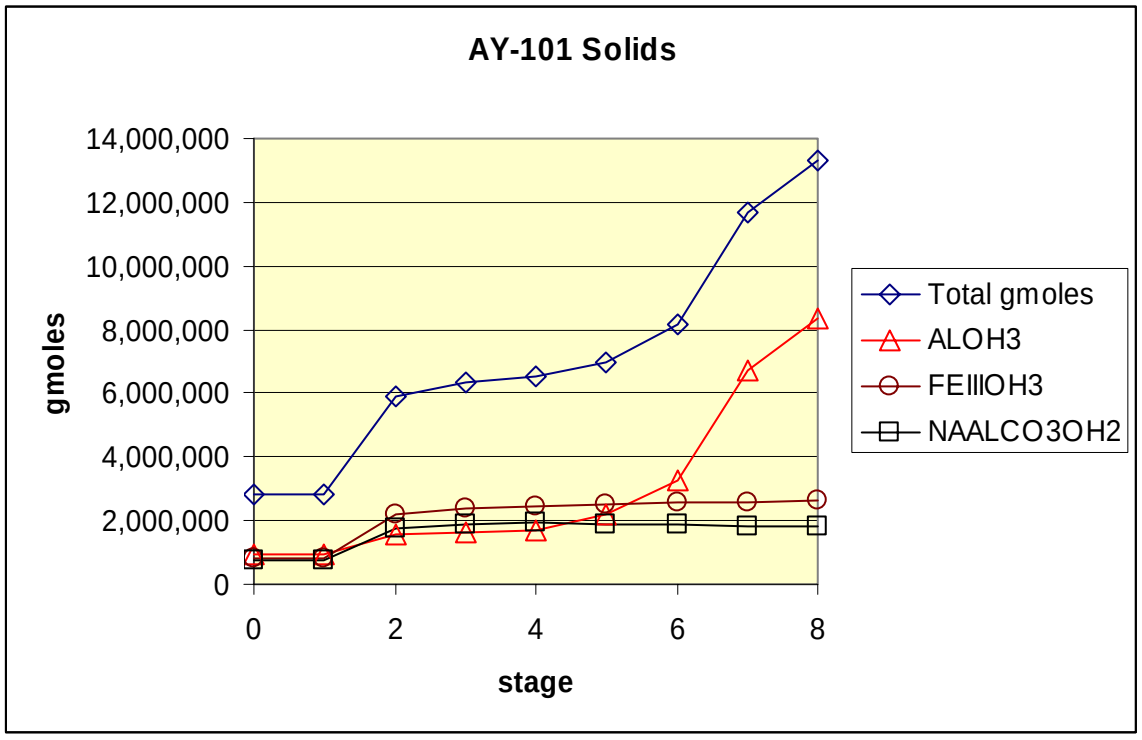

Figure 18 – AY-101 Solids (moles)

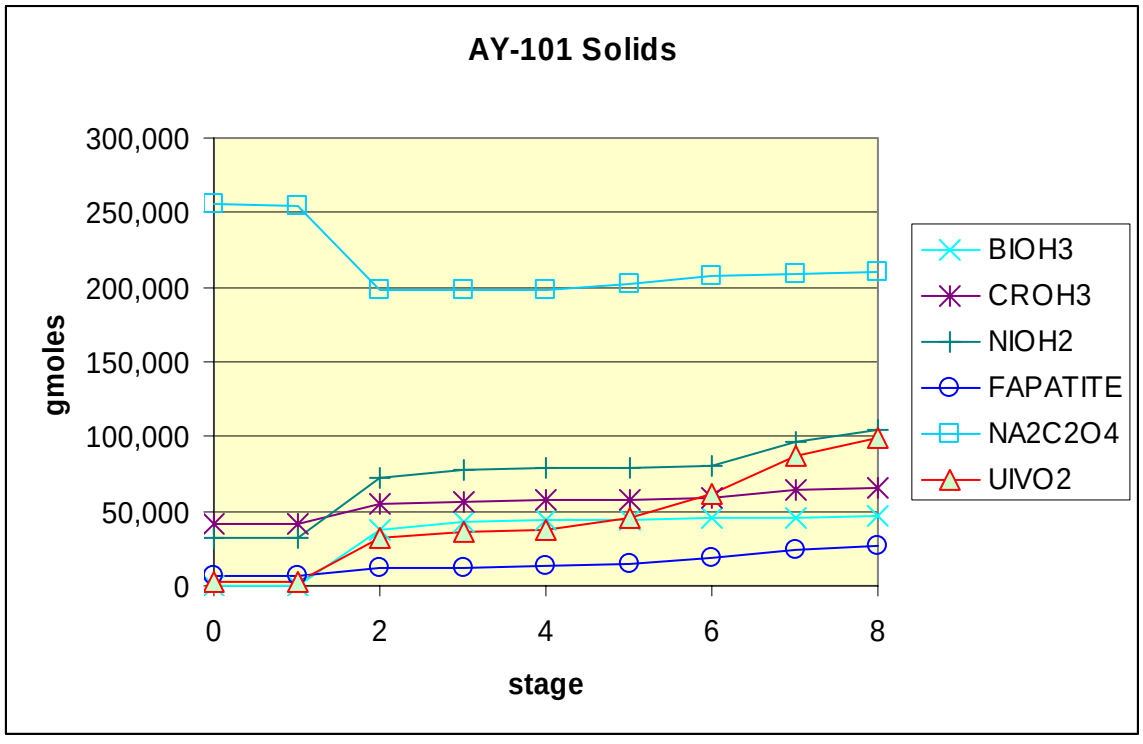

Figure 19 – AY-101 Solids (moles)

Table 7 – C tank Conditions During Retrieval Into AY-101

	stage	0	1	2	3	4
C-107 Tank Conditions	gallons	279,869	274,590	19,979	7,980	2,700
	specific gravit	1.37	1.37	1.94	1.93	1.98
	wt% solids	26.04	26.43	76.69	76.37	78.98
	vol% solids	11.83	12.04	59.81	59.43	63.01
	Na molarity	3.83	3.83	2.58	2.61	2.61
	pH	7.08	7.08	11.84	11.84	11.84
	wt% water	55.06	54.77			17.54

	stage	0	1	2
C-101 Tank Conditions	gallons	47,878	30,242	2,683
	specific gravi	1.84	1.79	1.89
	wt% solids	60.26	69.73	77.39
	vol% solids	48.75	54.56	62.37
	Na molarity	8.97	3.95	2.77
	pH	13.80	12.93	11.99
	wt% water	20.22	22.84	18.64

	stage	0	1	2
C-105 Tank Conditions	gallons	108,964	29,698	2,551
	specific gravi	1.88	1.88	2.03
	wt% solids	55.89	71.21	79.81
	vol% solids	41.77	53.45	64.47
	Na molarity	6.26	3.14	2.98
	pH	12.51	12.11	11.93
	wt% water	28.04	23.04	16.37

AZ-101

The C-102 waste tank is scheduled to be retrieved into AZ-101. Currently, it is the only C farm tank projected to be retrieved into AZ-101. This is probably due to the high volume and solids content C-102. The Modified Sluicing with Recycle (MSwR) method will be employed. As in prior simulations, this waste retrieval was modeled using the OLI ESP equilibrium program as reported previously [3,5].

Table 4 displays several parameters of AZ-101 during the complete retrieval of the C tanks. These same parameters for the flush stream that is returned to the AZ tank are also displayed. The stage numbers correspond with each stage of the process with the initial state listed as stage 0. Figures 20 and 21 display several of these parameters in chart form. Figures 22 and 23 graphically show conditions of the flush stream that is returned to AZ-101. Table 9 shows the amounts of several of the major solids which are collected and appear in AZ-101. Again, these solids are shown after each stage of the total retrieval process. Figures 24 and 25 show these major solids in chart form.

Table 10 shows the conditions present in C-102 during the retrieval process. Again, stage 0 is used to represent the initial conditions in the tank.

Table 8 – AZ tank and flush conditions during retrieval of C-102

			C-102			
	stage	0	1	2	3	4
	gallons	842,181	847,567	1,151,307	1,163,338	1,168,612
	specific gravit	1.25	1.25	1.34	1.35	1.35
AZ-101	wt% solids	4.55	4.54	16.00	16.68	17.07
Tank	vol% solids	2.17	2.16	8.41	8.80	9.03
Conditions	Na molarity	4.81	4.81	4.83	4.83	4.83
	pH	13.61	13.61	13.39	13.39	13.39
	wt% water	70.45	70.46	61.84	61.34	61.05
	stage		1	2	3	4
	gallons		5,402	1,534,107	268,278	586,452
Flush	specific gravi		1.28	1.30	1.26	1.24
Return to	wt% solids		2.15	9.99	4.21	1.09
AZ-101	vol% solids		1.09	5.12	2.09	0.53
	Na molarity		4.83	4.83	4.83	4.83
	pH		12.38	13.34	13.39	13.39
	wt% water		71.31	66.23		72.82

Table 9 – AZ-101 Solids during the Retrieval of C-102

AZ-101 Solids		C-102			
stage	0	1	2	3	4
Total gmoles	2,163,800	2,171,860	11,413,900	12,074,000	12,440,599
ALOH3	1,792,075	1,799,770	10,578,432	11,205,421	11,553,635
BIOH3	0	0	9,397	10,077	10,454
CROH3	42,721	42,729	53,226	53,976	54,392
FEIIIOH3	307,260	307,485	575,313	594,444	605,067
NIOH2	12,290	12,359	105,059	111,683	115,360
FAPATITE	3,220	3,241	31,207	33,205	34,314
NA2C2O4	0	0	0	0	0
NAALCO3OH2	0	0	0	0	0
UIVO2	6,235	6,276	61,266	65,195	67,377

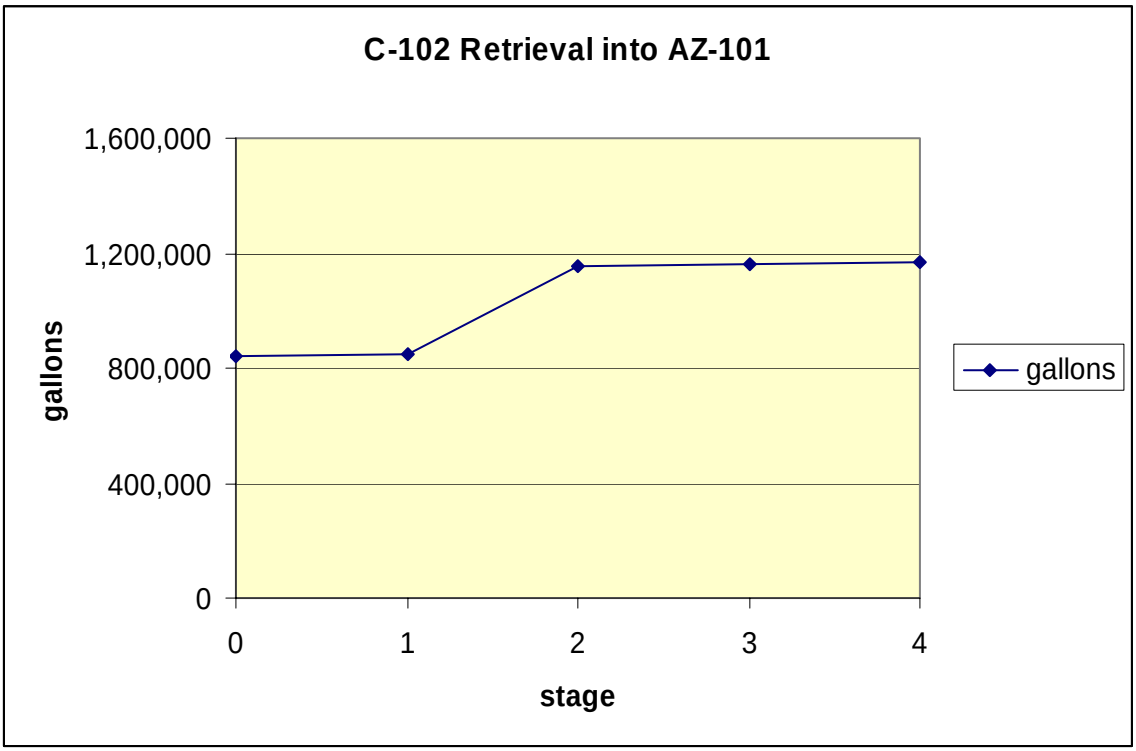

Figure 20– Total Volume of AZ-101 during retrieval of C tanks

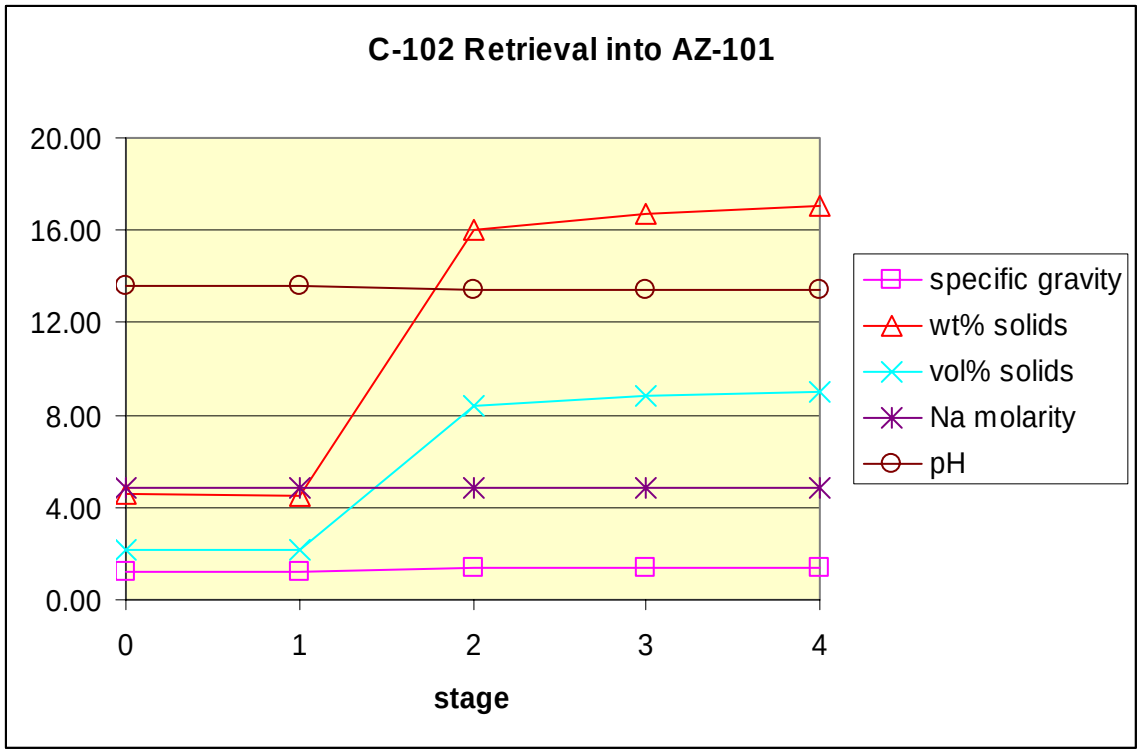

Figure 21 – AZ-101 Conditions During Retrieval of C tanks

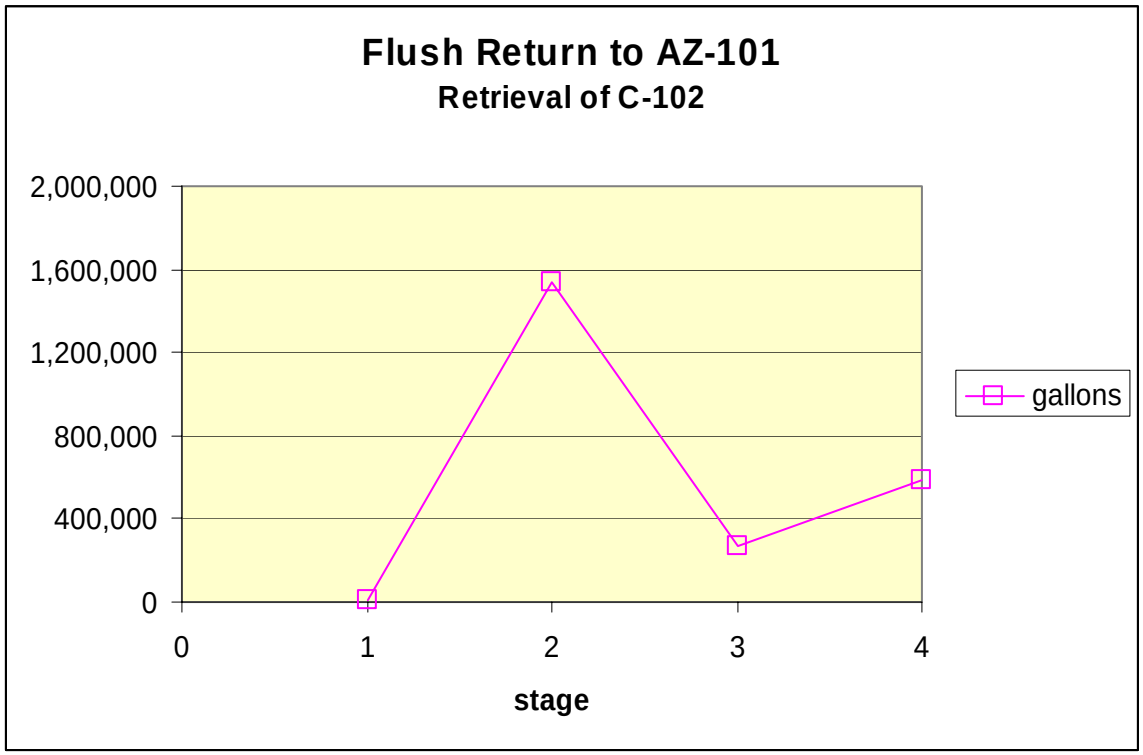

Figure 22 – Total Volume of Flush Stream to AZ tank

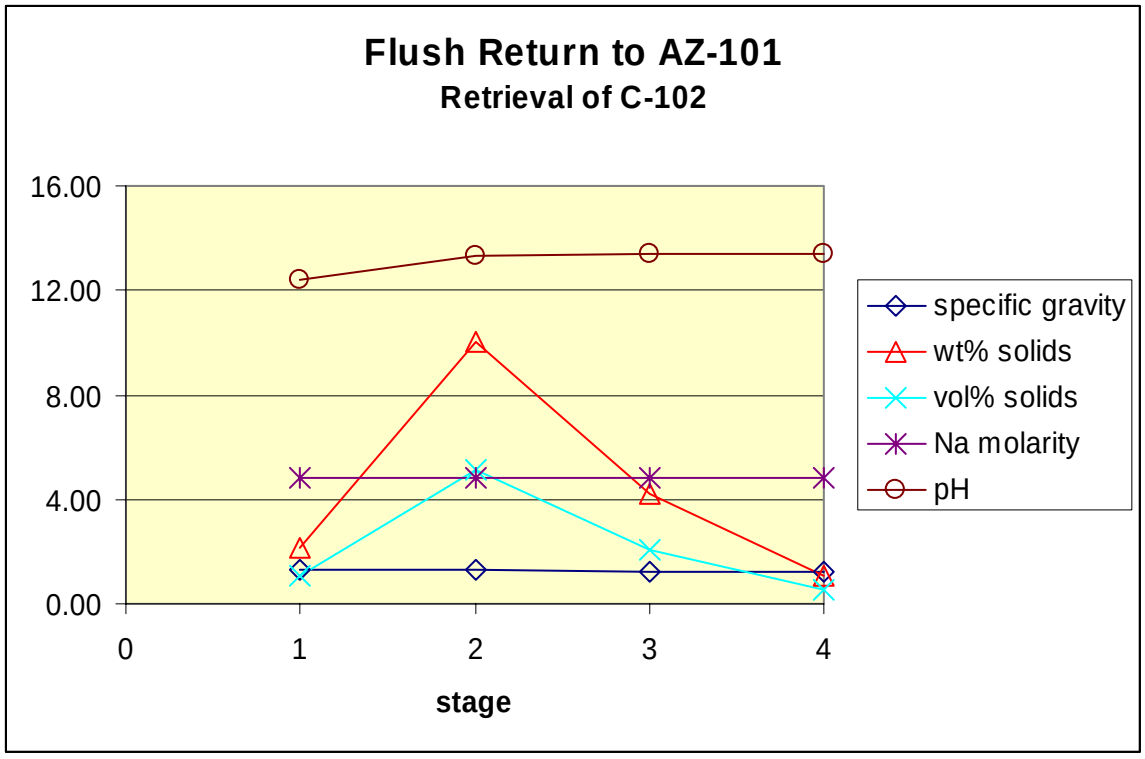

Figure 23 – Conditions of Flush Stream to AZ tank

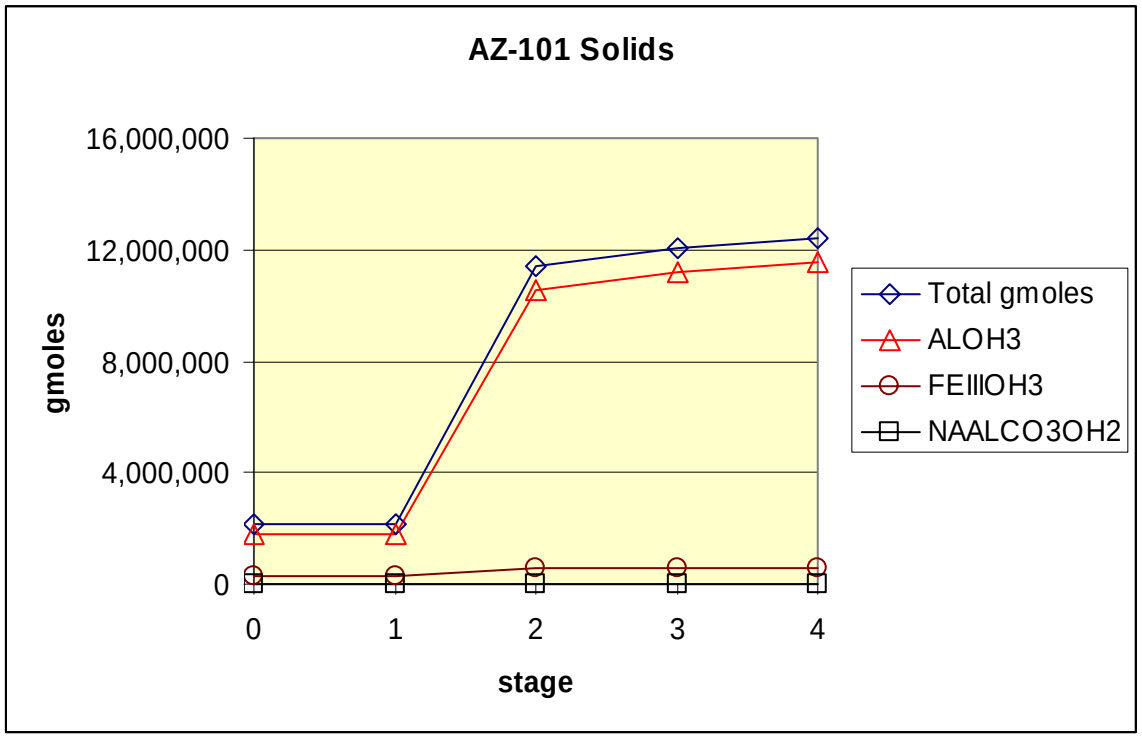

Figure 24 – AZ-101 Solids (moles)

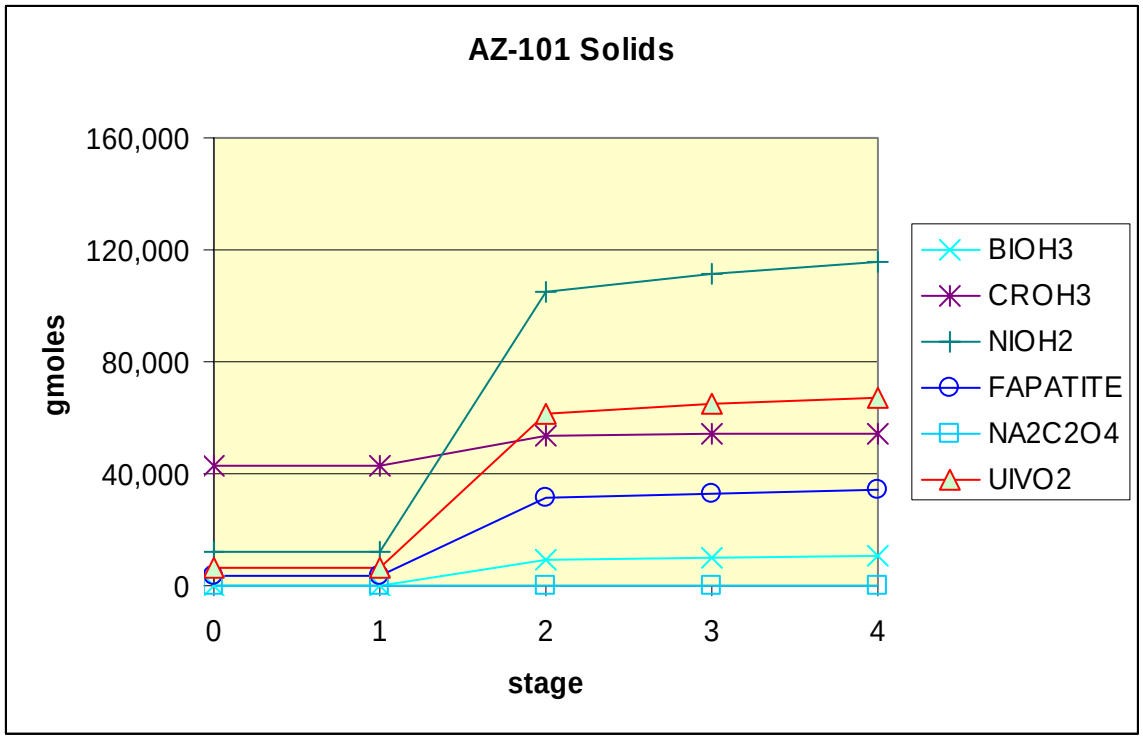

Figure 25 – AZ-101 Solids (moles)

Table 10 – C tank Conditions During Retrieval Into AZ-101

	stage	0	1	2	3	4
	gallons	329,698	324,300	19,926	7,898	2,627
	specific gravit	1.61	1.62	1.91	2.03	2.07
C-102	wt% solids	42.47	43.00	69.24	76.10	78.55
Tank	vol% solids	26.93	27.36	52.20	60.70	63.99
Conditions	Na molarity	4.83	4.83	4.83	4.83	4.83
	pH	12.38	12.38	13.39	13.39	13.39
	wt% water	41.93	41.54			15.79

C Tank Low pH

During the simulation of the retrieval of C-104, C-112, and C-111 into AN-101 which was reported previously [6], it was noticed that the C-111 tank composition after input into the ESP thermodynamic simulation program reflected an initial C tank pH value which was lowered than anticipated. The pH calculated by the ESP program was 5.58, which was much lower than that anticipated. Discussion with Hanford personnel concurred that the pH in the C farm tanks should meet or exceed 9.0 in all cases. It was also suggested by Hanford personnel to increase the NaOH content of the C tank to raise the pH to at least 9.0. Table 11 shows the changes in the C-111 initial composition that were made to determine the effect on pH.

Table 11 – C-111 Initial Composition Change as NaOH is Increased

	orig		110% Na	normalized		120% Na	normalized
H2O	6.65E-01		6.65E-01	6.61E-01		6.65E-01	6.57E-01
ACET2	2.02E-04		2.02E-04	2.01E-04		2.02E-04	1.99E-04
ALOH3	1.24E-01		1.24E-01	1.23E-01		1.24E-01	1.23E-01
BIOH3	9.06E-04		9.06E-04	9.00E-04		9.06E-04	8.94E-04
CAOH2	1.17E-02		1.17E-02	1.16E-02		1.17E-02	1.16E-02
CROH3	1.83E-04		1.83E-04	1.82E-04		1.83E-04	1.80E-04
CSOH	1.63E-07		1.63E-07	1.62E-07		1.63E-07	1.61E-07
FEiiiOH3	2.78E-02		2.78E-02	2.76E-02		2.78E-02	2.74E-02
H2CO3	1.13E-02		1.13E-02	1.13E-02		1.13E-02	1.12E-02
H2SO4	1.52E-03		1.52E-03	1.51E-03		1.52E-03	1.50E-03
H3PO4	1.88E-02		1.88E-02	1.87E-02		1.88E-02	1.86E-02
H4SIO4	8.03E-03		8.03E-03	7.98E-03		8.03E-03	7.93E-03
H6F6	7.52E-04		7.52E-04	7.47E-04		7.52E-04	7.42E-04
HCL	8.45E-04		8.45E-04	8.40E-04		8.45E-04	8.34E-04
HNO2	2.13E-02		2.13E-02	2.12E-02		2.13E-02	2.10E-02
HNO3	3.06E-02		3.06E-02	3.04E-02		3.06E-02	3.02E-02
KOH	6.62E-04		6.62E-04	6.58E-04		6.62E-04	6.54E-04
NaOH	6.42E-02		7.06E-02	7.02E-02		7.70E-02	7.61E-02
NiOH2	9.77E-03		9.77E-03	9.70E-03		9.77E-03	9.64E-03
Oxalac	8.97E-05		8.97E-05	8.91E-05		8.97E-05	8.86E-05
SROH2	7.58E-05		7.58E-05	7.53E-05		7.58E-05	7.48E-05
UivOH4	2.09E-03		2.09E-03	2.07E-03		2.09E-03	2.06E-03

Table 12 shows ESP predicted values for several C-111 parameters as the NaOH level is increased according to Table 11. As is seen in Table 12, an increase of 20% in the amount of NaOH present in C-111 only raised the pH value to 6.3. In addition, there does not seem to be significant changes in the mole fractions of the components shown.

Since, according to Tables 11 and 12, the NaOH level in C-111 would need to be significantly increased above the best basis reported values, and since we do not currently have a basis for adjusting components other than NaOH, it was determined to simulate all C farm tanks without any adjustments due to ESP generated pH values.

Table 12 – C-111 Initial Composition Change as NaOH is Increased

original		
Stream	c111i solids	c111i solids
Phase	Aqueous	Solid
Temperature,	30	30
Pressure, atm	1	1
pH	5.58503	
Total mol/hr	8466650	1493510
Flow Units	molefrac	molefrac
H2O	0.864849	
ALOH3	3.06E-11	0.681569
BIOH3	1.15E-07	0.005503
CACO3	1.23E-13	
FEIIIOH3	3.65E-10	0.168897
NANO3	0.001278	
NIOH2	3.95E-12	
OXALAC	3.15E-16	
SIO2	1.85E-05	0.04868
H2PO4ION	0.00663	
NAION	0.054059	
NIION	0.008681	
UIVOH3ION	2.49E-16	
UIVOH5ION	2.36E-16	
FAPATITE		0.014216
UIVO2		0.012698
NAALCO3OH2		0.068437
Total kg/hr	187339	143411
Volume, L/hr	152437	52316.8
Enthalpy, cal/h	-5.86E+11	-4.7E+11
Density, kg/L	1.22896	2.7412
Vapor fraction		
Solid fraction		1
Organic fractio		
Osmotic Pres,	147.83	
Redox Pot, vo		
Ionic Strength	5.70582	

110% Na normalized		
Stream	c111i solids	c111i solids
Phase	Aqueous	Solid
Temperature,	30	30
Pressure, atm	1	1
pH	6.23762	
Total mol/hr	8.50E+06	1.49E+06
Flow Units	molefrac	molefrac
H2O	0.859961	
ALOH3	2.82E-11	0.677746
BIOH3	1.06E-07	0.005467
CACL2	2.21E-29	
FEIIIOH3	3.37E-10	0.167777
NANO3	0.001239	
NIOH2	5.19E-11	0.005846
OXALAC	2.20E-17	
SIO2	1.71E-05	0.048361
H2PO4ION	0.002572	
NAION	0.060254	
NIION	0.008041	
UIVOH3ION	5.78E-17	
UIVOH5ION	1.07E-15	
FAPATITE		0.014122
UIVO2		0.012613
NAALCO3OH2		0.068069
Total kg/hr	187427	143323
Volume, L/hr	151988	52188.9
Enthalpy, cal/h	-5.88E+11	-4.68E+11
Density, kg/L	1.23318	2.74623
Vapor fraction		
Solid fraction		1
Organic fractio		
Osmotic Pres,	147.549	
Redox Pot, vo		
Ionic Strength	6.27463	

120% Na normalized		
Stream	c111i solids	c111i solids
Phase	Aqueous	Solid
Temperature,	30	30
Pressure, atm	1	1
pH	6.33708	
Total mol/hr	8.46E+06	1.51E+06
Flow Units	molefrac	molefrac
H2O	0.856845	
ALOH3	2.87E-11	0.666408
BIOH3	1.07E-07	0.005347
CACL2	1.80E-29	
FEIIIOH3	3.42E-10	0.163885
NANO3	0.001346	
NIOH2	5.28E-11	0.023959
OXALAC	2.15E-17	
SIO2	1.74E-05	0.047328
H2PO4ION	0.002343	
NAION	0.066565	
NIION	0.005164	
UIVOH3ION	4.55E-17	
UIVOH5ION	1.30E-15	
FAPATITE		0.013876
UIVO2		0.012321
NAALCO3OH2		0.066875
Total kg/hr	185654	145096
Volume, L/hr	151242	52543.7
Enthalpy, cal/h	-5.86E+11	-4.69E+11
Density, kg/L	1.22753	2.76143
Vapor fraction		
Solid fraction		1
Organic fractio		
Osmotic Pres,	160.313	
Redox Pot, vo		
Ionic Strength	6.13021	

WORK FORECAST

This report concludes the simulation of all scheduled C farm tank retrievals using the ESP simulation models for the modified sluicing with recycle (MSwR) method and the mobile retrieval system (MRS) method. Work is in progress to generate the neural network training set data using this complete set of C farm ESP process simulations. The results of neural network development will be detailed in a subsequent report.

CONCLUSIONS

An ESP process simulation model, which approximates the C tank farm Modified Sluicing with Recycle (MSwR) and the Mobile Retrieval System (MRS) for waste retrieval has been used to evaluate the retrieval of C-107, C-101, and C-105 waste into AY-101. Further simulations have evaluated the retrieval of C-102 into AZ-101. In addition, the pH predicted by the ESP simulation program based on the initial best basis values for C farm tanks was found to be significantly lower than the value of 9.0 given by Hanford personnel as a minimum. It was determined that the level of NaOH needed to increase the pH to the minimum of 9.0 was too high to be undertaken without further justification from Hanford. As such, all C farm tank retrieval simulations were performed without adjustments to best basis values for predicted low C tank initial pH values.

REFERENCES

1. Toghiani, R. K., Phillips, V. A., and Lindner, J. S., "Solubility of Na-F-SO_4 in Water and in Sodium Hydroxide Solutions," Journal of Chemical and Engineering Data 50(5), 1615, (2005).

2. Selvaraj, D. K., (2003), Solubility Studies in the Na-F-PO_4 System in Sodium Nitrate and in Sodium Hydroxide Solutions, MS Thesis, Chemical Engineering, Mississippi State University, Mississippi State, MS.

3. Lindner, J.S., Luthe, J.C., Pearson, L.E., Smith, L.T., Toghiani, R.K., (2007), "Process Chemistry and Operations Planning for Hanford Waste Alternatives" in "Accelerating Cleanup of the Defense Nuclear Legacy," ICET Quarterly Technical Progress Report for the period July 1 - September 31, 2007, Report Number 07040R03 U. S. Department of Energy Agreement Number DE-FC01-06EW-07040, Mississippi State, MS.

4. Larry Wall, Tom Christiansen, Jon Orwant, "Programming Perl," Third Edition, O'Reilly, Sebastopol, CA 2000.

5. Lindner, J.S., Luthe, J.C., Pearson, L.E., Smith, L.T., Toghiani, R.K., (2008), "Process Chemistry and Operations Planning for Hanford Waste Alternatives" in "Accelerating Cleanup of the Defense Nuclear Legacy," ICET Quarterly Technical Progress Report for the period April 1, - June 30, 2008, Report Number 07040R06 U. S. Department of Energy Agreement Number DE-FC01-06EW-07040, Mississippi State, MS.

6. Lindner, J.S., Luthe, J.C., Pearson, L.E., Smith, L.T., Toghiani, R.K., (2008), “Process Chemistry and Operations Planning for Hanford Waste Alternatives” in “Accelerating Cleanup of the Defense Nuclear Legacy,” ICET Quarterly Technical Progress Report for the period July 1, - September 30, 2008, Report Number 07040R07 U. S. Department of Energy Agreement Number DE-FC01-06EW-07040, Mississippi State, MS.

Task 5

Phytoremediation and Long-Term Monitoring of Heavy Metal Contaminants

Yi Su, Fengxiang Han, and David Monts

INTRODUCTION

Previous studies on phytoremediation of heavy metals have been focused on terrestrial plants. However, aquatic plants could also be potential candidates for phytoremediation of contaminated water and phytofiltration of collective storm water and surface runoff.

WORK ACCOMPLISHMENT

Green House experiments with mercury contaminated water and water lettuce (*Pistia stratiotes*) has been conducted to study Hg uptake and phytotoxicity. Our preliminary results show that water lettuce effectively removed Hg from solutions with initial Hg concentrations of 1, 5, and 10 mg/L (Fig. 26.). After 1 day of plant growing, 93-99% of Hg as HgCl2 was removed from water. After 7 days, Hg in all solutions was under the detection limit.

The leaves and roots of the plants were collected and prepared for chemical analysis. Mercury concentration in solution, plant shoots and roots were analyzed by ICP-AES (inductively coupled plasma-atomic emission spectrometry) and CVAAS (cold vapor atomic absorption spectrometry). Most of Hg was stored in roots (up to 25000 mg/kg dry weight base) (Fig. 27). Hg concentrations in shoots and roots linearly increased with the increase of Hg concentrations in solutions.

Hg shows acute toxicity to water lettuce indicated by a decrease in fresh weight biomass and relative leaf water content (Fig. 28).

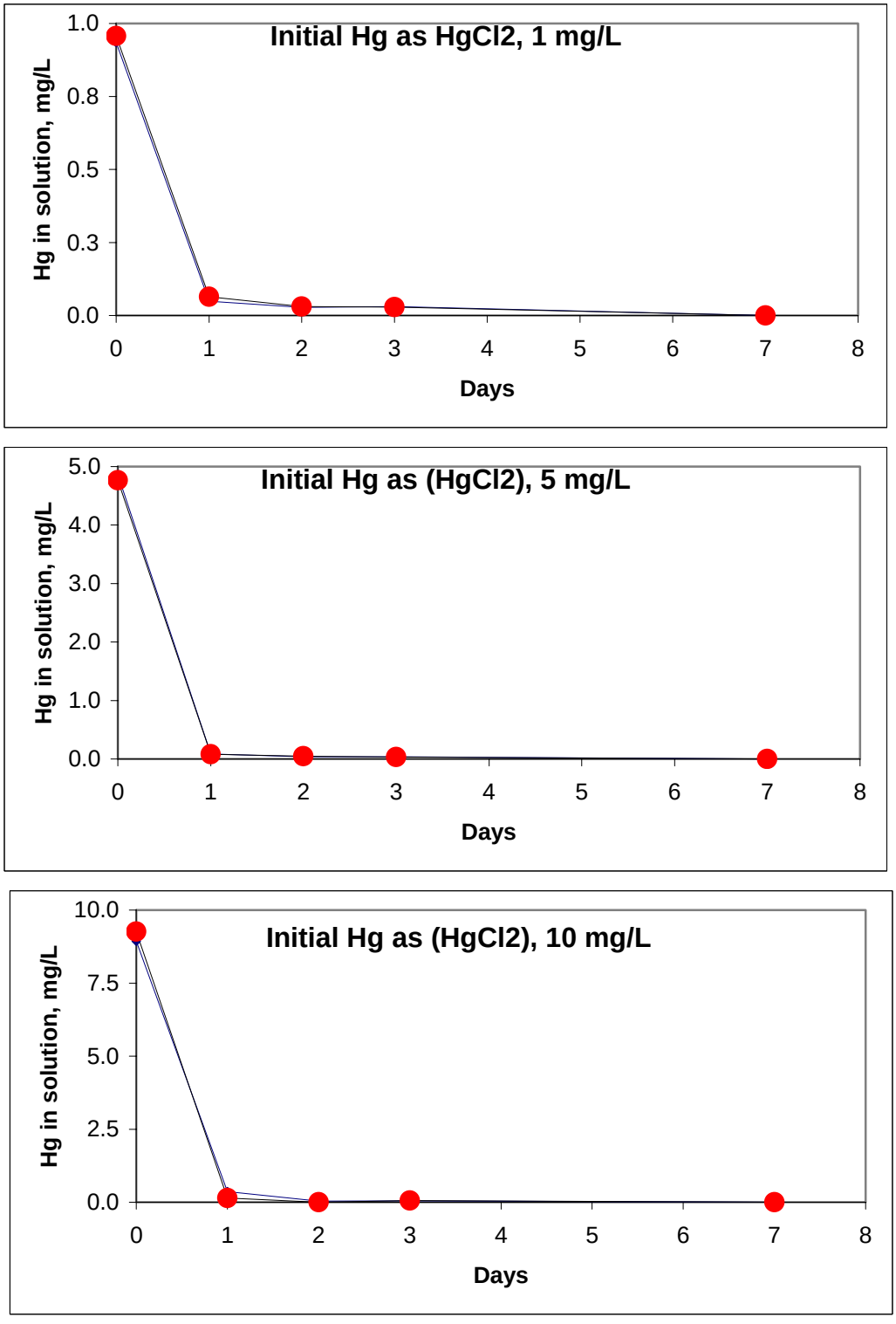

Figure 26. Kinetics of Hg uptake by water lettuce from solutions with initial Hg concentrations from 1 to 10 mg/L.

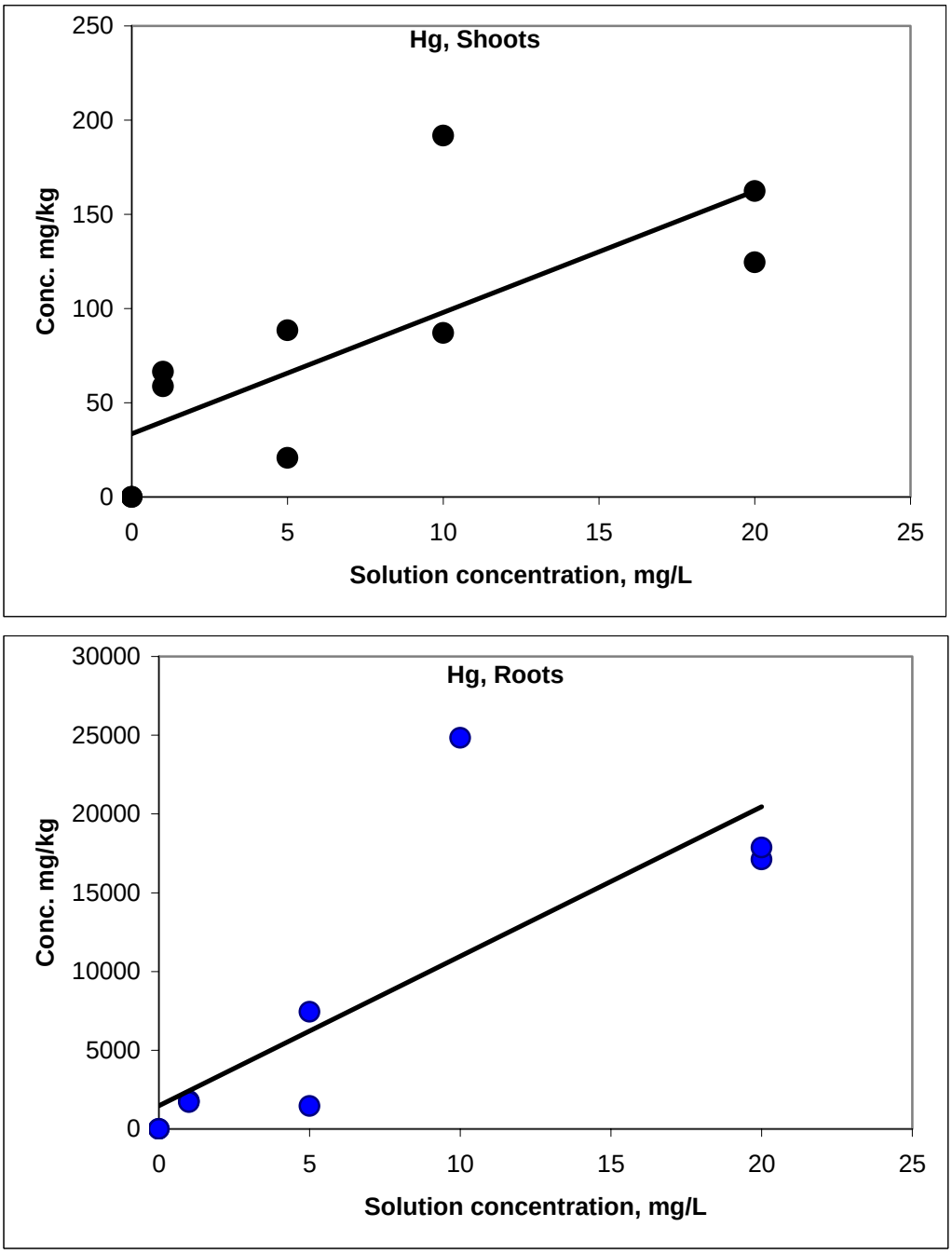

Figure 27. Hg concentrations in shoots and roots as a function of initial Hg concentrations in solution.

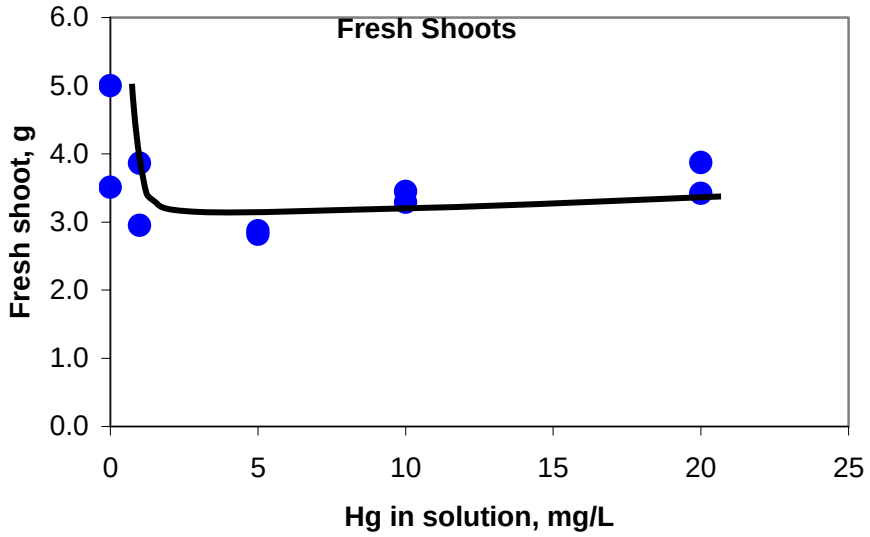

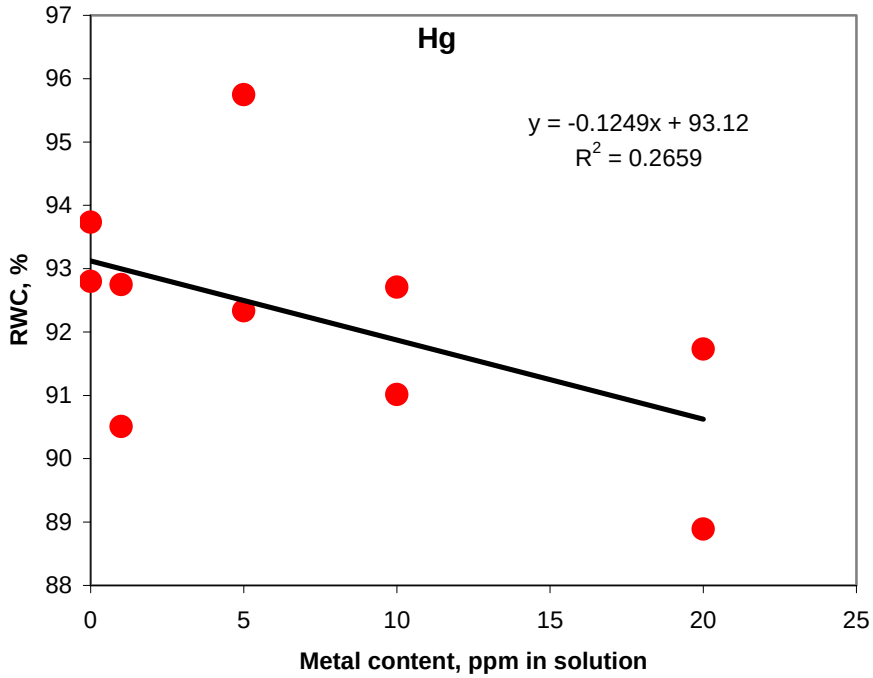

Figure 38. Effects of Hg on fresh weight of shoots and relative water contents.

CONCLUSION

The preliminary results indicate that water lettuce can effectively remove Hg from contaminated solutions, but the phytotoxicity is acute. Further systematic studies are needed to evaluate the phytoremediation potential for this aquatic species. Mercury lost via evaporation will also be evaluated in future studies.

WORK PLANNED

Greenhouse studies on phytoremediation application of aquatic plants for mercury and other heavy metals Are continuing.

Task 6

Saltstone

Ronald Palmer and R. Arunkumar

INTRODUCTION

This project is comprised of two subtasks. The first consists of laboratory scale experiments designed to examine the thermal properties of new Saltstone formulations. The second consists of Pilot Scale studies.

Laboratory Scale Experiments

Small batches prepared in the laboratory must be done prior to designing the pilot scale tests. Lab methods will be set up for measuring the heat of hydration for various Saltstone formulations.

Mixers capable of providing batches from as small as several 10s of grams to more than one kilogram are available in the ICET laboratory. A standard protocol for making these small batches will be developed.

An adiabatic calorimeter will designed and built to measure the heat of hydration of the Saltstone formulations. This device will provide basic thermal property measurements. These data are important contributions to new revisions of the Performance Assessment documentation.

Pilot Scale Studies

Small batches prepared in the laboratory can only provide preliminary information. A pilot-scale facility, capable of producing 55-gallon drum sized product, is available at the ICET laboratories. Drums can be appropriately instrumented to examine the heat generation of Saltstone formulations on an intermediate scale between the laboratory and actual Saltstone production facility.

Using these same waste simulant recipes, various formulations of Saltstone will be produced at our pilot-scale facility. The laboratory scale work provides the basis for determining which formulations to study further. The results of this work will provide the confidence necessary for full scale production at the Saltstone production facility.

WORK ACCOMPLISHED DURING THIS QUARTER

To demonstrate and analyze the performance of the control system on the calorimeter, initial tests of the apparatus were performed during this quarter. To enhance the control system, an amplifier was installed to boost the differential thermocouple temperature measurements between the cement sample and the surrounding bath. One long test of the calorimeter was performed.

For this test, a cement water mixture (46% water, 54% Portland cement, by weight) was utilized. A 718g cement sample was poured into a PVC container weighing approximately 500g. This sealed container along with two thermocouples (Type T) for measuring an absolute and a differential temperature were placed inside a Dewar flask in the calorimeter. An inverted Dewar flask was placed over this and the whole assembly was placed inside the calorimeter.

Two thermocouples (Type T) to measure the absolute and differential temperature of the water bath were also connected to the control/measurement system. An on/off power controller that operated off the differential thermocouple measurement was the prime control element to the system. A secondary part of the control system was a variac supplying the actual power to the heating element placed in the bottom of the calorimeter bath. (For this experiment, the calorimeter was operated without a stirrer. We have since added a variable speed stirrer to the bath.)

The test was operated over a 120-hour period and none of the systems failed. Results from this test are shown in the charts below. The first chart shows the gradual rise in temperature of the cement and the water bath. The second chart shows the temperature difference between the sample (cement) temperature and the controlled water bath temperature. Once the initial stabilization of the bath temperature was accomplished, the controller tracks the sample temperature to within 0.4^{o} C over the entire test period of 120 hours.

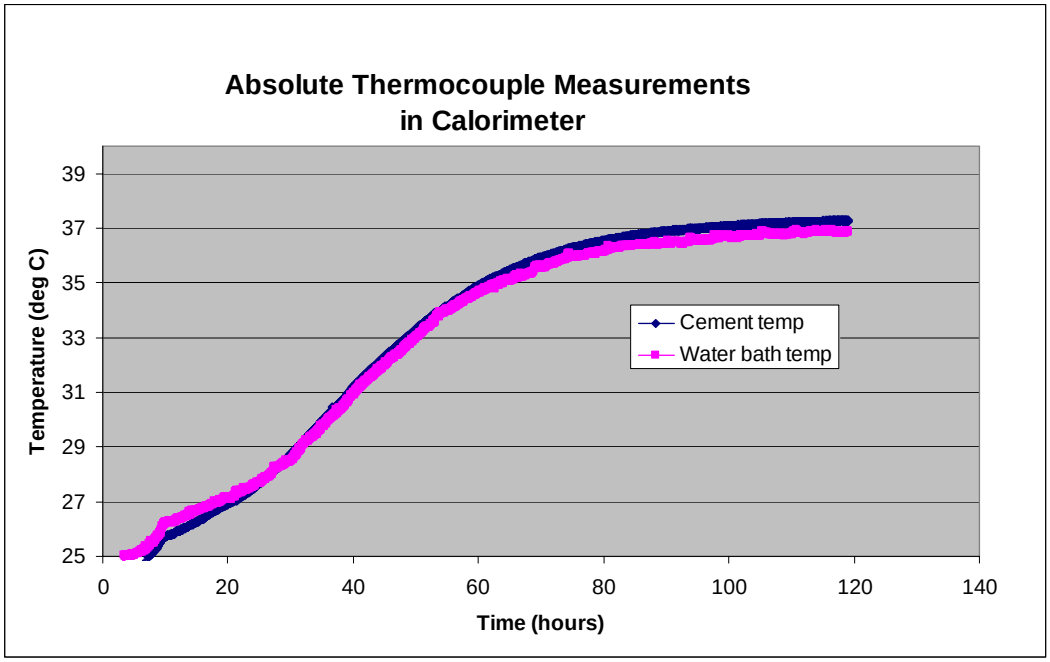

Figure 29. Absolute thermocouple measurements in calorimeter

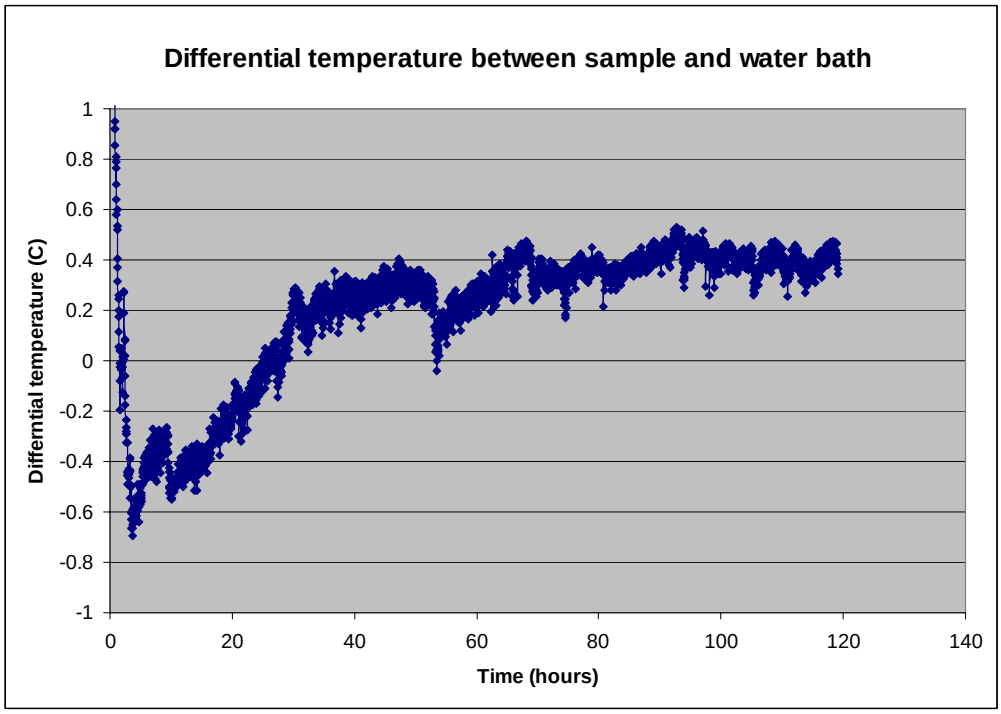

Figure 30. Differential temperature between sample and water bath

Other work in the laboratory during this reporting period included:

- Designing experiments with 1kg batches studying the heat evolution of the Saltstone formulations using containers outfitted with thermocouples
- Continued working toward a test plan due March 31
- Continue to experiment with the protocol for making salt solutions and small batches of Saltstone formulations, including using water in place of the salt solution
- Obtained the SRNL design for a thermocouple tree for measuring thermal behavior in pilot scale system and work toward its assembly and prepare for an possible pilot scale tests in later 2009
- Investigate the possibility of adding a modeling task to this activity

WORK FORECAST FOR NEXT QUARTER

The following tasks are expected to be active during the next quarter:

- Continue to experiment with the protocol for making salt solutions and small batches of Saltstone formulations, including using water in place of the salt solution
- Complete the construction of an adiabatic calorimeter and run initial experiments using water/cement mixtures
- Investigate the possibility of adding a modeling task to this activity
- Investigate the possibility of using our Differential Scanning Calorimeter for making specific heat measurements
- Continued working toward a test plan due March 31

REFERENCES

1. Steimke, J. L. and M. D. Fowley, "Measurement of Thermal Properties of Saltstone," WSRC TR-97-00357, Westinghouse Savannah River Company, Aiken, SC, 1997.
2. Harbour, J. R. et al., "Characterization of Slag, Fly Ash and Portland Cement for Saltstone," WSRC-TR-2006-00067, Revision 0, Savannah River National Laboratory, Aiken, SC, 2006.
3. Harbour, J. R. et al., "Heat of Hydration of Saltstone Mixes – Measurement by Isothermal Calorimetry," WSRC-STI-2007-00263, Revision 0, Savannah River National Laboratory, Aiken, SC, 2007.
4. Lee, Si Young, "Thermal Performance Analysis for WSB Drum," WSRC-STI-2008-00262, Savannah River National Laboratory, Aiken, SC, May 2008.
5. Cozzi, A. D., et al., "Effect of Heat of Hydration on Drum Temperature and Filter Performance in Full-Scale Waste Solidification Building Simulated High Cactivity Waste Drums," WSRC-STI-2008-00367, Revision 0, Savannah River National Laboratory, Aiken, SC, September 2008.

Task 7

Bioavailability Studies of Mercury and other Heavy Metal Contaminants in Ecosystems of Selected DOE Sights

Fengxiang X. Han, Yi Su, David L. Monts, and Charles A. Waggoner

Introduction

Previous studies indicated Fe/Mn oxides increased Hg solubility and the release of soluble mercury from HgS contaminated soil. It was also found that the increase in Cl concentrations in soils and subsurface resulted in increasing the release of SO_4, iron, and mercury as accompanied by the significant decrease in pH in both pure HgS system and HgS contaminated Oak Ridge soils when they were reacted with Fe oxides, especially magnetite. However, the effect of pH change on this process has not been documented.

Work Accomplishments

The effects of initial pH on release of SO_4 from pure HgS after reacting with Fe_3O_4 increased with pH, while it is not significant in the HgS + Fe_2O_3 system (Fig. 31). However, Fe release decreased with the increase in the initial pH due to precipitation and adsorption of Fe at higher pH. Pure HgS system did not have any pH buffer capacity, but both Fe_2O_3 and Fe_3O_4 had a strong pH buffer capacity to counter initial pH changes (Fig. 32). Further, the pH values in pure HgS with both Fe oxides were slightly lower than pure Fe oxide systems (Fig. 32).

The effects of initial pH on oxidation of HgS from Oak Ridge contaminated soils were studied. The results showed that pH did not significantly affect the rate of oxidation process of HgS by two iron oxides in Oak Ridge soils as indicated by release of SO_4 (Fig. 33). Only magnetite treatment slightly increased release of SO_4 from the contaminated soils. The final pH of contaminated Oak Ridge soils, after reacting with two iron oxides, were similar regardless of the initial pHs (4.0-8.0) (Fig. 34). This indicates that Oak Ridge contaminated soil had a strong pH buffer capacity to counter initial pH changes. One unit change of initial pH had a rough unit of

net pH change in the soils, resulting in the similar final pHs of soils among various initial pHs treatments (Fig. 5).

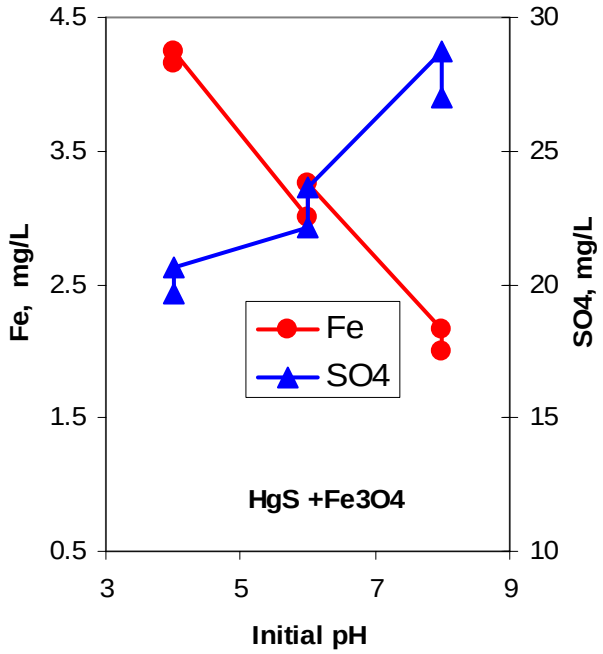

Figure 31. Effects of initial pH on SO_4 and Fe release from pure HgS after reacting with Fe_3O_4 (1 g Fe oxide, 0.1 g HgS, 35 ml 0.01M $NaNO_3$ at pH 4.0, 6.0 and 8.0 for 24 hrs).

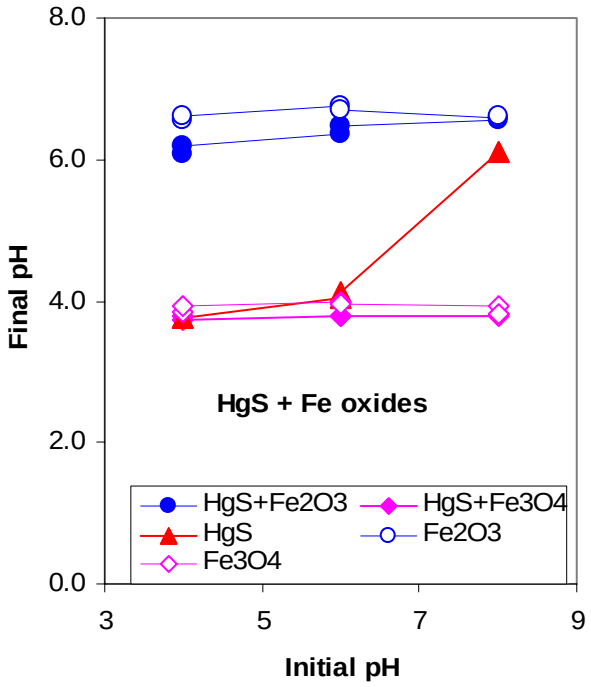

Figure 32. Final pH of pure HgS systems and HgS +Fe oxides at various initial pHs (conditions as the same as Fig. 1)

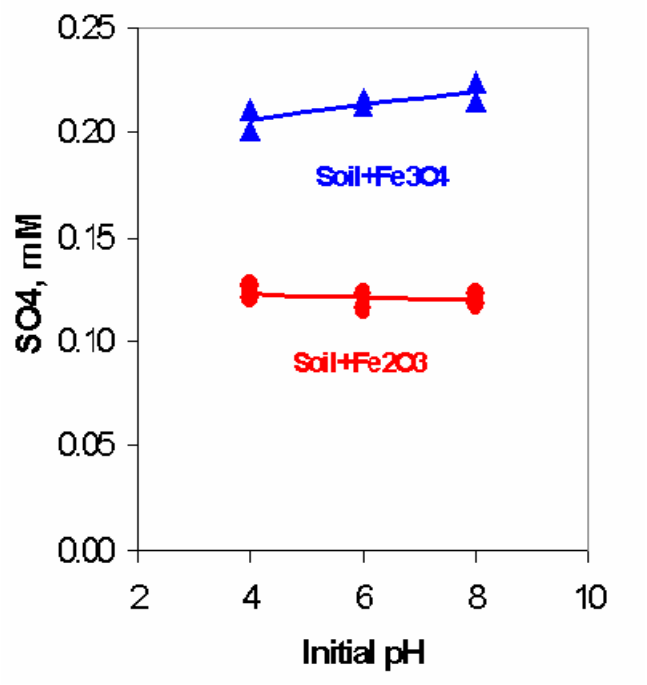

Figure 33. Effect of initial pH on sulfate release from Hg contaminated Oak Ridge soil (with 2000 mg/kg Hg as HgS) (5 g soil, 0.25 g Fe oxide, 35 ml 0.01M $NaNO_3$ at pH 4.0, 6.0 and 8.0 for 24 hrs).

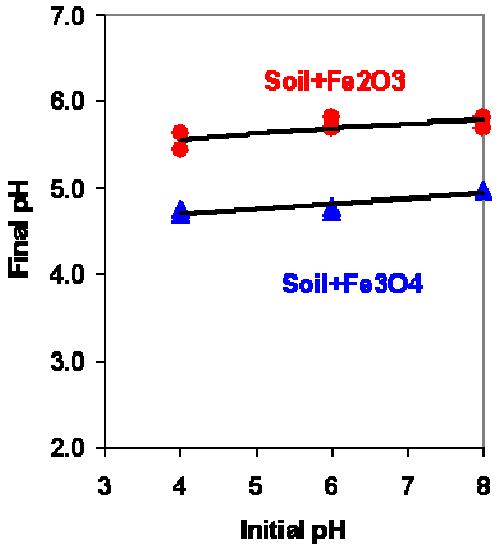

Figure 34. Final pH of contaminated HgS Oak Ridge soils with two iron oxides under various initial pH (4.0-8.0) conditions.

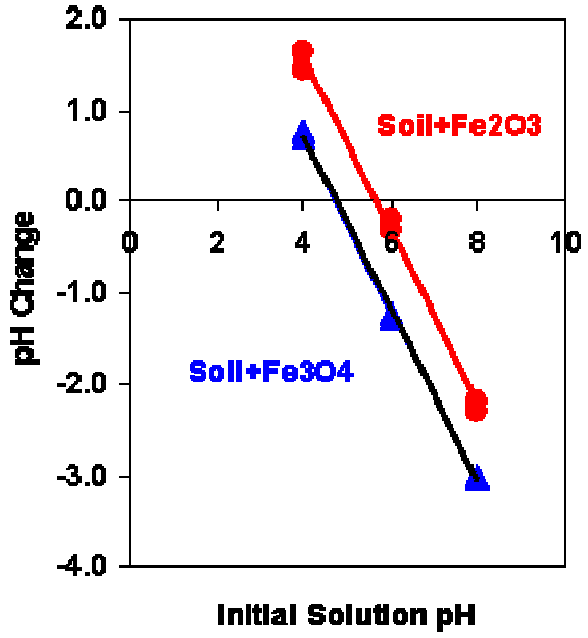

Figure 35. The net pH changes of contaminated soils after reacting with two iron oxides under various initial pHs.

Conclusions

The present study shows that pH did not significantly affect the rate of oxidation process of HgS by two iron oxides in Oak Ridge soils as indicated by release of SO_4, but the increase in pH did increase SO_4 release from pure HgS after reacting with Fe_3O_4. Magnetite and hematite in Oak Ridge contaminated soil had strong pH buffer capacity to counter initial pH changes, but pure HgS system did not have any pH buffer capacity.

Work Planned for Next Quarter

The effects of other environmental factors such as redox changes, dissolved organic carbon, and rhizosphere chemistry on the potential oxidation of HgS as indicated by the release of SO_4 from both pure HgS and contaminated soils will be studied.

IN-TANK CHARACTERIZATION FOR CLOSURE OF HANFORD WASTE TANKS

David L. Monts

INTRODUCTION

The goal of this project is to develop and deploy in-tank waste characterization tools for use at the Hanford Site. These will be used to reduce uncertainties and risks associated with waste processing and closure activities. Some of the systems developed for this effort are also applicable to other DOE sites, such as the Savannah River Site.

After as much waste as practical has been removed from the tank, analyses of remaining deposits will be needed to determine the long-term risk associated with the residual waste and to determine the appropriate steps required for closure. These needs are described in Hanford Technical Challenges WT-115, Technology to Support Post-Retrieval Evaluation of SSTs and also in the DOE-EM Engineering & Technology Roadmap, Improve Residual Waste Tank Characterization and Stabilization.

ICET is to assemble and test the following systems for potential deployment for nondestructive, *in situ* imaging means of quantitatively determining the volume and height of waste (including that deposited on tank walls, and the volume and depth of sediments), based on Fourier-transform profilometry (FTP) and stereovision (SV). FTP images are obtained by using a white light source to project a fringe pattern onto the object of interest and using a camera to record the resulting distortions of the fringe pattern due to reflection from non-flat surfaces. A software package has been developed by ICET that automatically processes the FTP image to yield quantitative measurements and renderings of the object. In some cases, tank solids are covered by a layer of pipeline flush water, following the completion of retrieval. Quantitative mapping of tank sediments would enable a more accurate determination of the volume of residual tank wastes. Sediment mapping is not feasible with currently deployed instrumentation. FTP will evaluate the feasibility of sediment mapping under a variety of conditions. Stereovision also provides 3-D topographical reconstruction of target surfaces by using images simultaneously recorded by two or more cameras from different viewpoints. (The Stereovision effort is currently frozen because of budget limitations).

WORK ACCOMPLISHED:

FOURIER TRANSFORM PROFILOMETRY

At the end of the first quarter, ICET was informed that because of the downward revision of the ICET Cooperative Agreement CA08 budget, that there are no funds to support the Hanford in-tank characterization effort for the current Cooperative Agreement year. ICET administrators subsequently issued a stop-work order. The bi-weekly conference calls with our Hanford collaborators were suspended. As a result of fund relocation from the FY08 ICET Cooperative Agreement, limited funds became available in September to perform a technical feasibility study for the Fourier profilometry (FTP) technique. This study and the report that will result were requested by our Hanford collaborators.

During this reporting period, FTP experiments were performed in the ICET highbay at distances and at angles of view that pertain to Hanford waste tanks. The 200-series Hanford waste tanks are typically ~75' in diameter with an internal height of ~38'5". An FTP probe would be deployed through a 4" inside diameter (I.D.) riser located 9' off center. The most challenging location at which to determine residual waste volumes is the "junction" where the upright wall joins the tank floor diametrically opposite the riser. If the FTP system is 25' above the tank bottom, then the far "junction" is ~52.8' away at an angle of ~62° from the vertical. Therefore, we have experimentally determined our ability to quantitatively determine the volume of non-descript objects located ~53' from our FTP system at angle of ~62°. The experiments were performed in ICET's high bay area with the lights off, as shown in Fig. 36. Three different non-descript targets from our previous development efforts were utilized and each was recorded in four different rotational configurations so that 12 independent determinations of volume were made. The "true" volumes of the non-descript targets were determined independently by traditional (volume-displacement) methods with a relative uncertainty of ~1%. Figure 36 also presents an example of the images acquired and a view of the prototype FTP setup used for the technical feasibility study.

The results for a camera-to-projector distance of 46.1 cm are presented in Table 13. The overall average measurement error is 5.2%. There is some variation in error from target to target: the smallest target (S6) had the largest average relative error (7.2%), followed by the largest target (S3) with 6.0% average error, and the middle-size target (S4) with the smallest average error (2.4%). Figure.37 shows photographs of these three non-descript targets. S6 is a "circular" target with sloping edges that is flattened on top. S4 is a "rectangular" target with sloping edges that is "rounded" at the top. S3 has the most irregular geometry, consisting of two "circular" "piles" joined together.

As noted above, the height determination is most sensitive to the separation d between the camera and the projector (after determination of phase shift). Therefore, we have investigated the effect of camera-to-projector distance d upon the volume measurement error; the results are summarized in Table 14. The results show an alternation of the sign of the error with d, but that once d has been set; all the errors have the same sign. This suggests a systematic error whose origin we are in the process of investigating. The results are consistent with a decrease in the

average error with increasing camera-to-projector distance d, as is predicted by the sensitivity analysis. The magnitude of the error decreases with decreasing target volume. Consequently, the relative error should be independent of volume. Table 15 shows that there is no obvious pattern for the relative error as a function of volume; this is not inconsistent with the relative FTP volume error being independent of volume. Fig. 38 shows that the magnitude of the average error decreases with increasing camera-to-projector distance d.

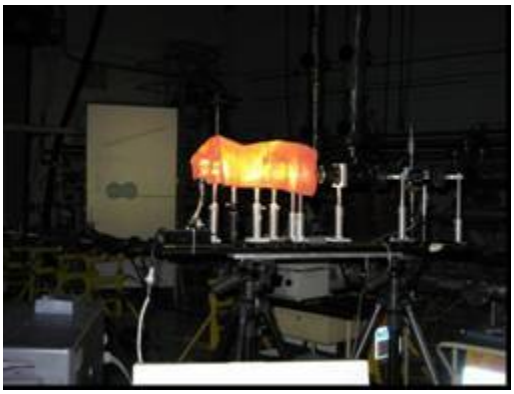

(a.)

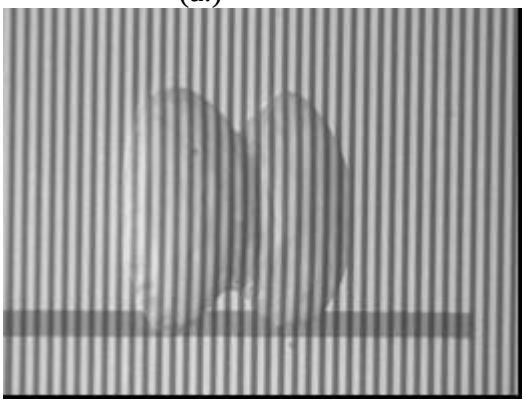

(b.)

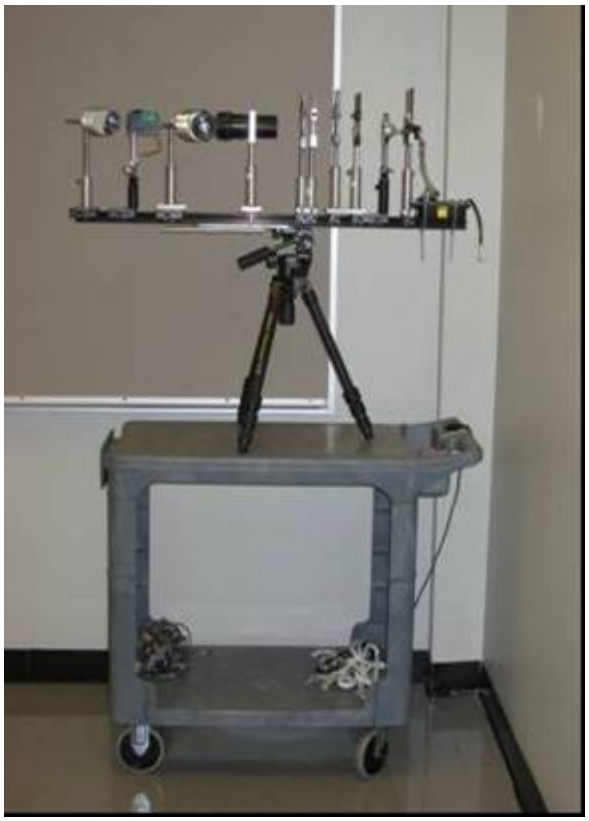

(c.)

Figure 36. (a) Photograph of ICET FTP components on optical rail viewing non-descript, grey targets on white background at distance of 16.2 m (53') and angle of ~62°. A cloth shroud has been placed over the light source to minimize the amount of non-fringe pattern light on the target. (b) Example image of a non-descript target with fringe lines projected on its surface, acquired using the setup in (a). (c) ICET FTP components on optical rail as utilized in the setup in (a).

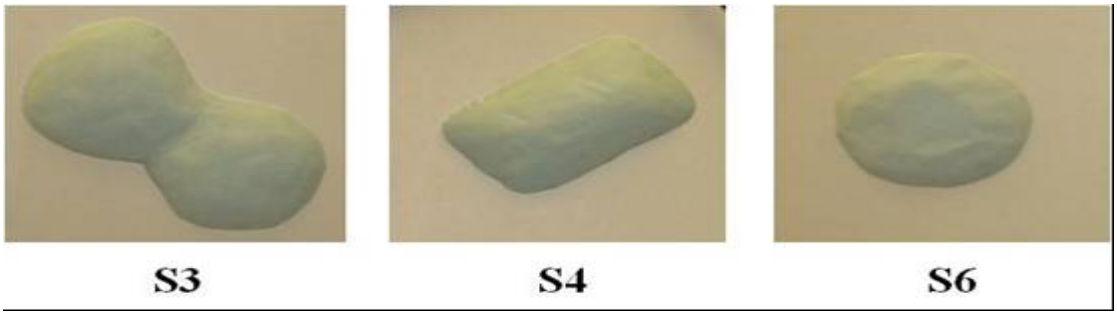

Figure 37. Photographs of the three non-descript targets used.

Table 13. Comparison of FTP-determined ("measured") and true volumes for three different non-descript targets. Each target was recorded in four different rotational orientations. The separation between camera and projector was 46.1 cm (~18").

Target	True Volume (cm^3)	Measured Volume (cm^3)	Error (cm^3)	Error (%)
S3	1954±10	2057	+103	+5.3
S3	1954±10	2039	+85	+4.4
S3	1954±10	2085	+131	+6.7
S3	1954±10	2105	+151	+7.7
S4	1071±6	1089	+18	+1.7
S4	1071±6	1129	+58	+5.4
S4	1071±6	1081	+10	+0.9
S4	1071±6	1087	+16	+1.5
S6	647±4	683	+36	+5.6
S6	647±4	686	+39	+6.0
S6	647±4	695	+48	+7.4
S6	647±4	711	+64	+9.9
Average				+5.2

Table 14. Comparison of average absolute errors for the selected non-descript targets as a function of the camera-to-projector distance ("baseline") d for d = 21.8 cm (~ 9"), d = 33.4 cm (~13"), and d = 46.1 cm (~18"). The uncertainties are one standard deviation. In the last column, the averages of the absolute values of the absolute errors are presented.

Target	True Volume (cm^3)	Error d=21.8 cm (cm^3)	Error d=33.4 cm (cm^3)	Error d=46.1 cm (cm^3)	Average
S3	1954±10	+221±57	-144±70	+118±29	161
S4	1071±6	+98±24	-108±19	+26±22	77
S6	647±4	+63±35	-38±25	+47±13	49

Average		+127	-97	+64	96

Table 15. Comparison of average relative errors for the selected non-descript targets as a function of the camera-to-projector distance ("baseline") d for d = 21.8 cm (~ 9"), d = 33.4 cm (~13"), and d = 46.1 cm (~18"). In the last column, the averages of the absolute values of the relative errors are presented.

Target	True Volume (cm^3)	Error d=21.8 cm	Error d=33.4 cm	Error d=46.1 cm	Average
S3	1954±10	+11.3%	-7.4%	+6.0%	8.2%
S4	1071±6	+9.1%	-10.0%	+2.4%	7.2%
S6	647±4	+9.8%	-5.9%	+7.2%	7.6%
Average		+10.0%	-7.8%	+5.2%	7.7%

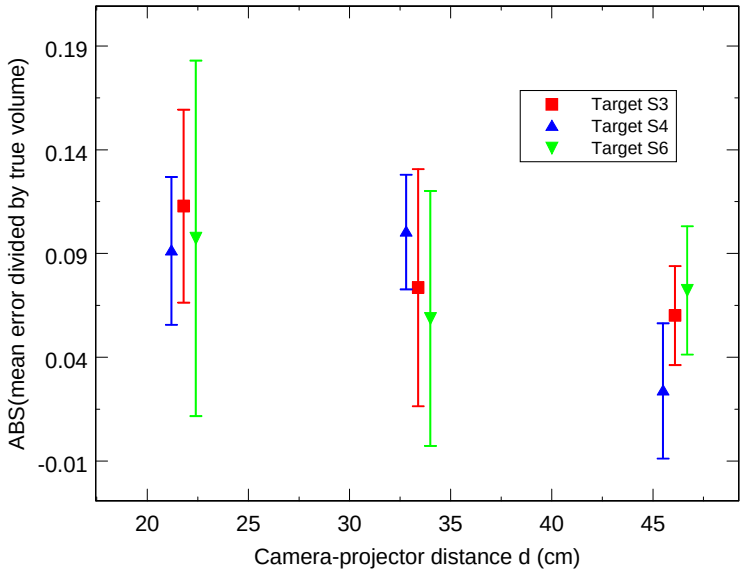

Figure 38. Plot of the magnitude of the average absolute error divided by the true volume (giving the average relative error) as a function of the camera-to-projector distance d. Horizontal dithering has been applied to the data to separate the data points and 95% confidence-limit error bars.

A draft of a conference paper describing the FTP technical feasibility study preliminary results has been prepared and submitted to the 2009 Waste Management conference [1].

WORK PLANNED

FOURIER TRANSFORM PROFILOMETRY

A series of experiments will be performed at ICET to identify and characterize the systematic error that is evident in Tables 14 and 15. Upon completion, the FTP technical feasibility report will be completed.

REFERENCES

1. David L. Monts, Ping-Rey Jang, Zhiling Long, O. Perry Norton, Walter P. Okhuysen, Yi Su, and Charles A. Waggoner, "Technical Performance Capability of Fourier Transform Profilometry for Quantitative Waste Volume Determination under Hanford Waste Tank Conditions," *Proceedings of 35th Waste Management Symposium (WM'09)*, March 1-5, 2009, Phoenix, AZ, Paper No. 9333.

ACRONYMNS

CTF	Cold Test Facility
FTP	Fourier transform profilometry
ICET	Institute for Clean Energy Technology
SV	stereovision